Nuclear pastas and superfluidity in neutron-star crusts

Nicolas Chamel
Université Libre de Bruxelles, Belgium

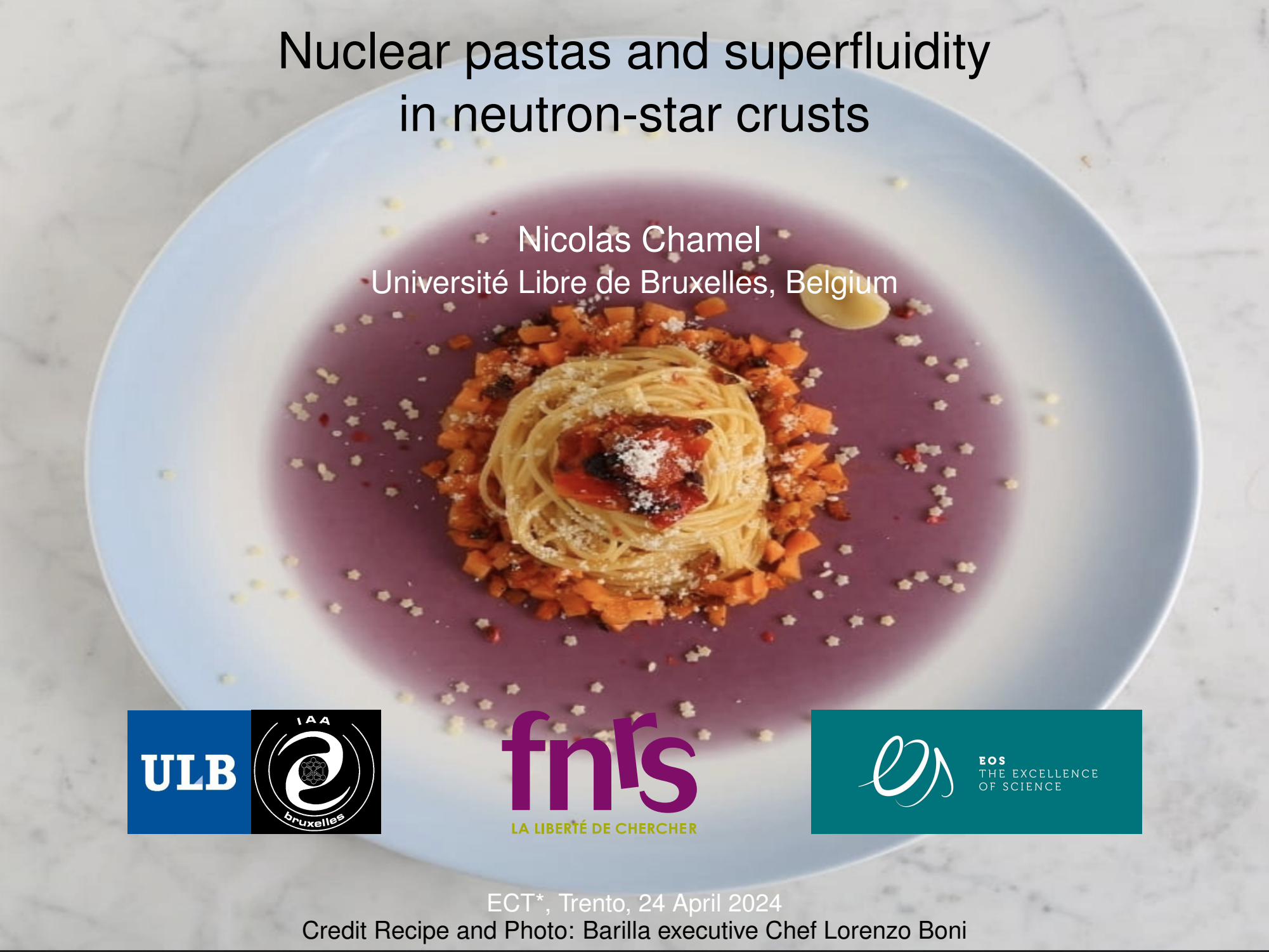

ECT*, Trento, 24 April 2024
Credit Recipe and Photo: Barilla executive Chef Lorenzo Boni

Neutron stars are cool

Formed in gravitational core-collapse supernova explosions, neutron stars are the **most compact stars** in the Universe.

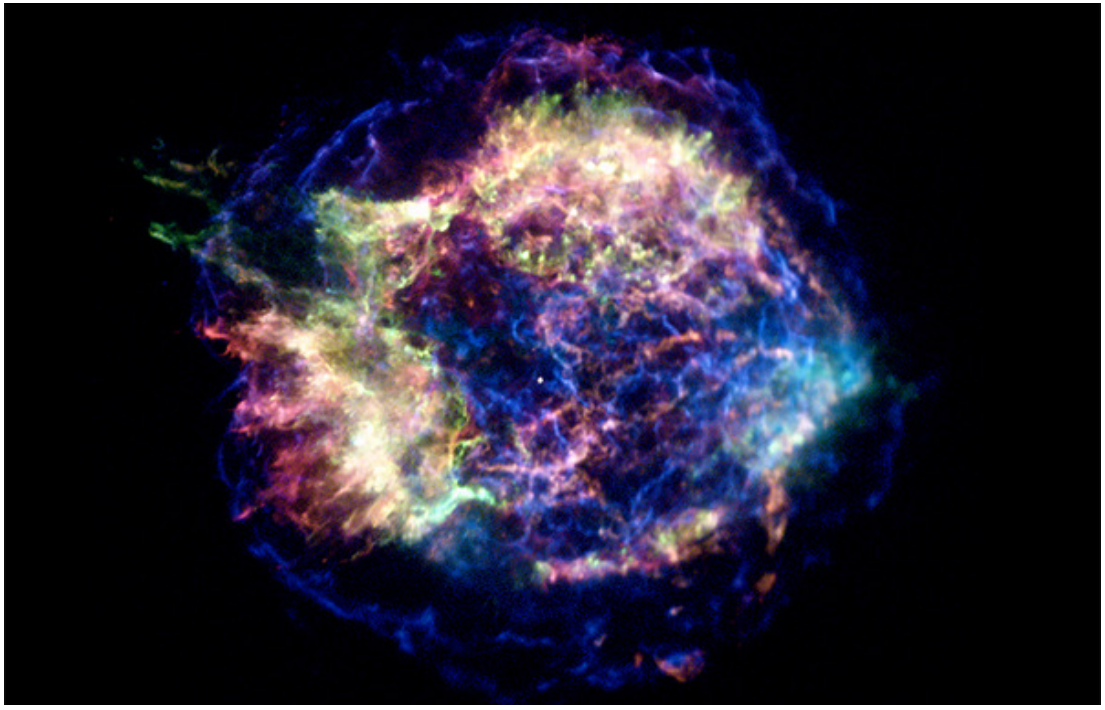

Nuclear physics:

$M \sim 1 - 2M_\odot$
$R \sim 10$ km
$\Rightarrow \rho \sim 10^{15}$ g cm^{-3}

Energy scale: MeV

"cold" $\lesssim 10^{10}$ K $\lesssim$ "hot"

Neutron stars are initially very hot ($\sim 10^{12}$ K) but cool down to $\sim 10^9$ K within days by releasing neutrinos.

Their dense matter is thus expected to undergo various phase transitions, as observed in terrestrial materials at low-temperatures.

Neutron star interior

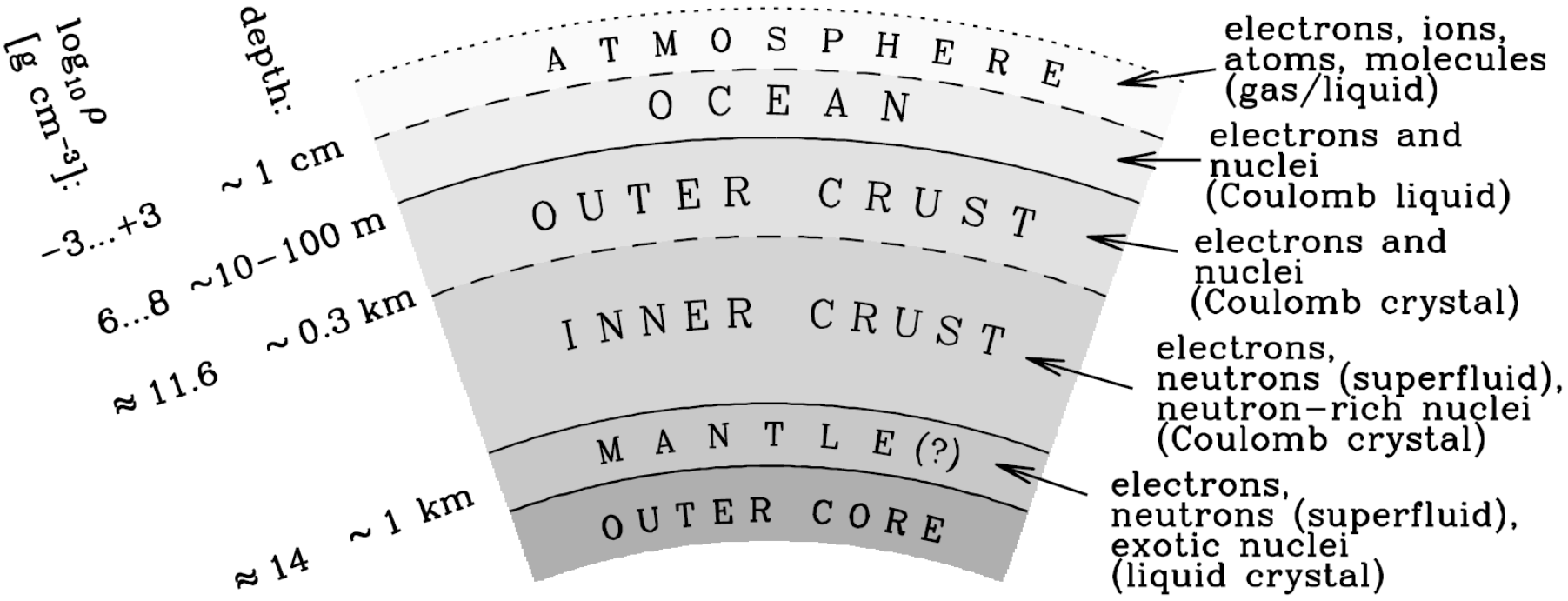

picture taken from Haensel, Potekhin, Yakovlev, "Neutron Stars" (Springer, 2007)

The mantle may consist of very exotic configurations so called nuclear "pastas" in a neutron superfluid.

Blaschke&Chamel, Astrophys. Space Sci. Lib. 457, eds L. Rezzolla, P. Pizzochero, D. I. Jones, N. Rea, I. Vidaña p. 337-400 (Springer, 2018), arXiv:1803.01836

Outline

1. Nuclear pastas in neutron stars
   - Semi-microscopic treatment
   - Role of quantum shell effects
2. Neutron superfluidity in neutron-star crusts
   - Small superflow: superfluid density
   - Large superflow: gapless superfluidity
   - Astrophysical applications
3. Conclusions & perspectives

Nuclear pastas in neutron star

Nuclei in dense stellar environments

Back in 1971, Baym, Bethe and Pethick showed within the liquid-drop picture that the existence of nuclei in dense matter arises from a **detailed balance between surface and Coulomb effects:**

$$E_{\rm surf} = 2E_{\rm Coul}$$

They anticipated that nuclei would become unstable at some point:

> The fraction of space, u, occupied by nuclei is seen in table 2 to increase monotonically until the nuclei begin to touch. For a bcc lattice the value $u = \sqrt{3}\pi/8 = 0.68$ corresponds to the nuclei just touching. The picture of nuclei as spherical drops is certainly not valid beyond this point. The nuclear parameters A, Z and $n_{\rm N}$, given for $\rho = 2.26 \times 10^{14}$ and 2.39×10^{14} g/cm^3 should be regarded as highly tentative since they are particularly sensitive to the precise way in which the surface energy tends to zero as $n_{\rm n}/n \to 1$. Furthermore, our model has neglected deformations of the nuclei, which become important here. In fact, it might be more favorable, beyond $u = 0.5$, for the nuclei to "turn inside out", that is, for the neutron gas to exist as a lattice of droplets in a sea of nuclear matter.

Baym, Bethe, Pethick, Nucl. Phys. A175, 225 (1971)

Nuclei in neutron-star crust vs ordinary nuclei

Solving the HF equations in spherical Wigner-Seitz cells in 1973, Negele&Vautherin found that both types of nuclei look similar:

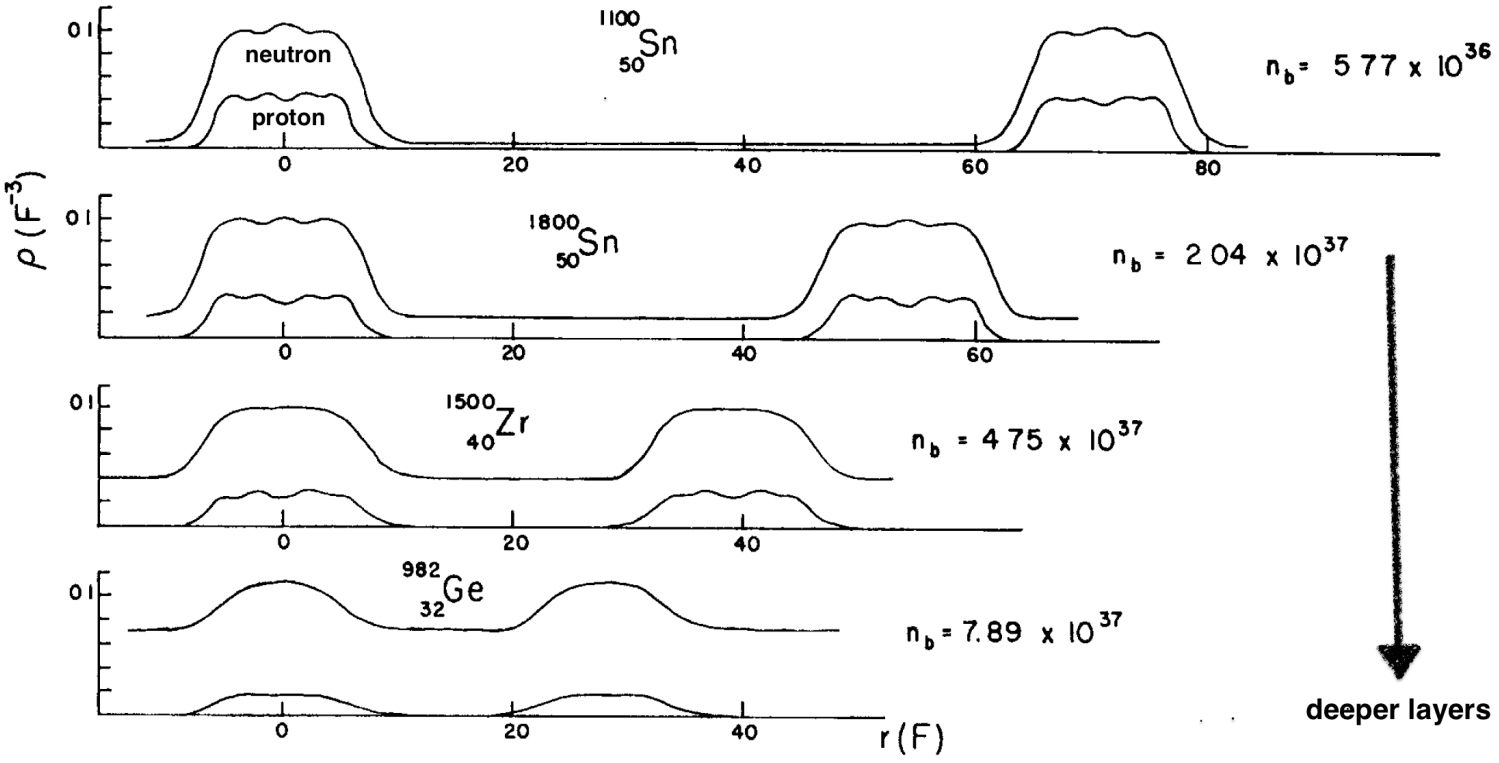

Negele&Vautherin,Nucl.Phys.A207,298(1973)

Nuclei in neutron-star crust vs ordinary nuclei

Solving the HF equations in spherical Wigner-Seitz cells in 1973, Negele&Vautherin found that both types of nuclei look similar:

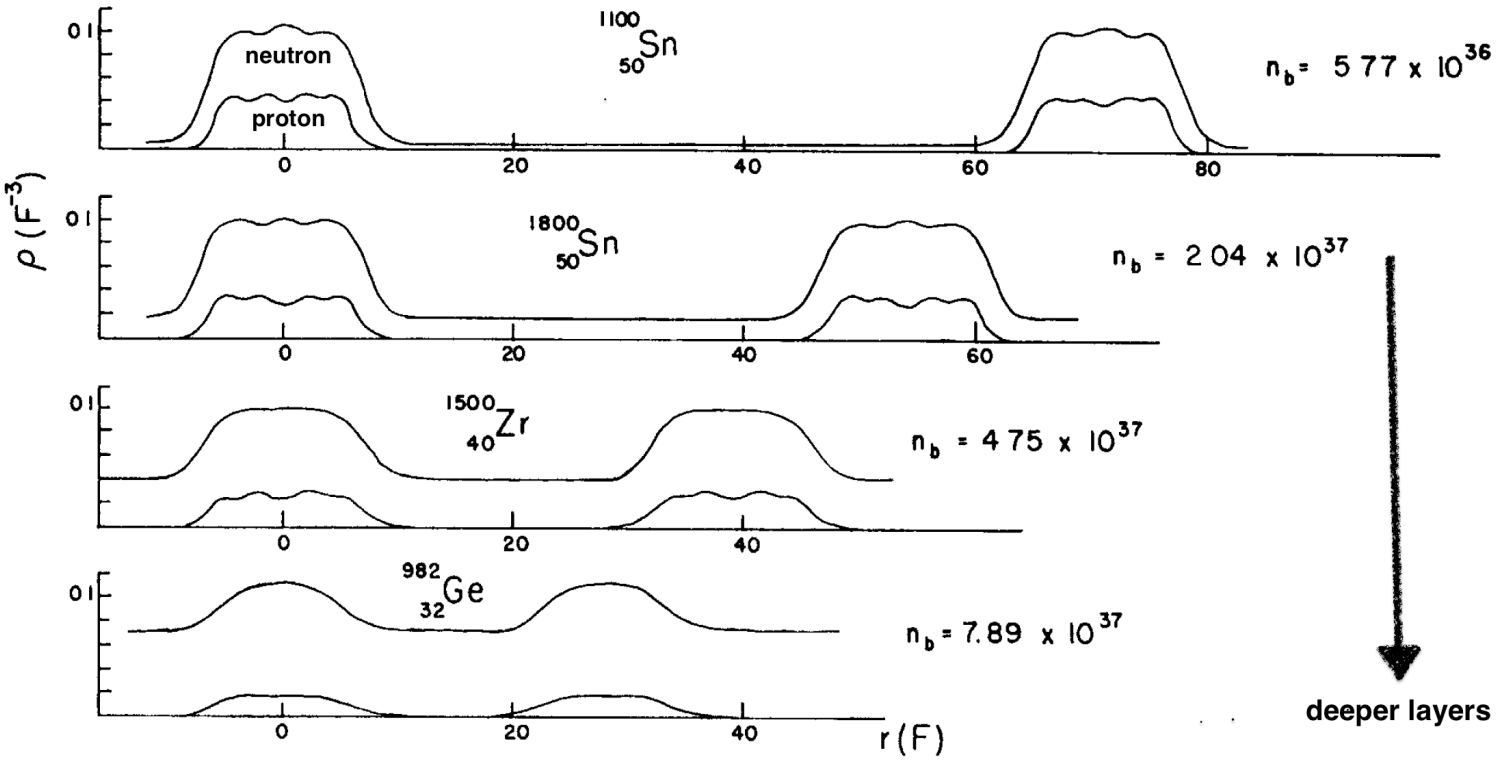

Negele&Vautherin,Nucl.Phys.A207,298(1973)

But they were not able to probe the existence of nuclear bubbles because of numerical instabilities.

Limitations of the Wigner-Seitz approach

The W-S approach is unreliable $\gtrsim 0.02$ fm^{-3} due to spurious shell effects induced by approximate boundary conditions.

Chamel et al, PRC75, 055806 (2007); Pastore et al, J.Phys.G44,094003 (2017)

Unbound neutron energy levels of zirconium isotopes with $N = 160$ (70 unbound) in a body-centered cubic lattice at $\bar{n} = 4 \times 10^{-4}$ fm^{-3}:

W-S approximation

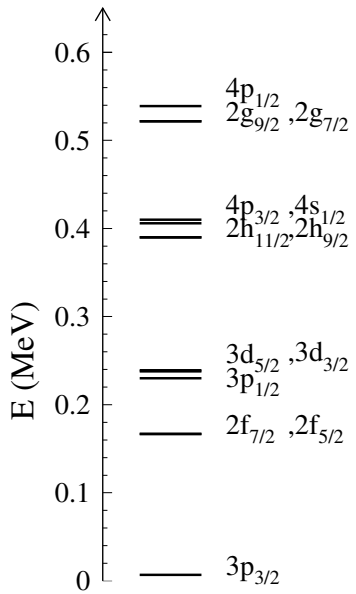

band theory of solids

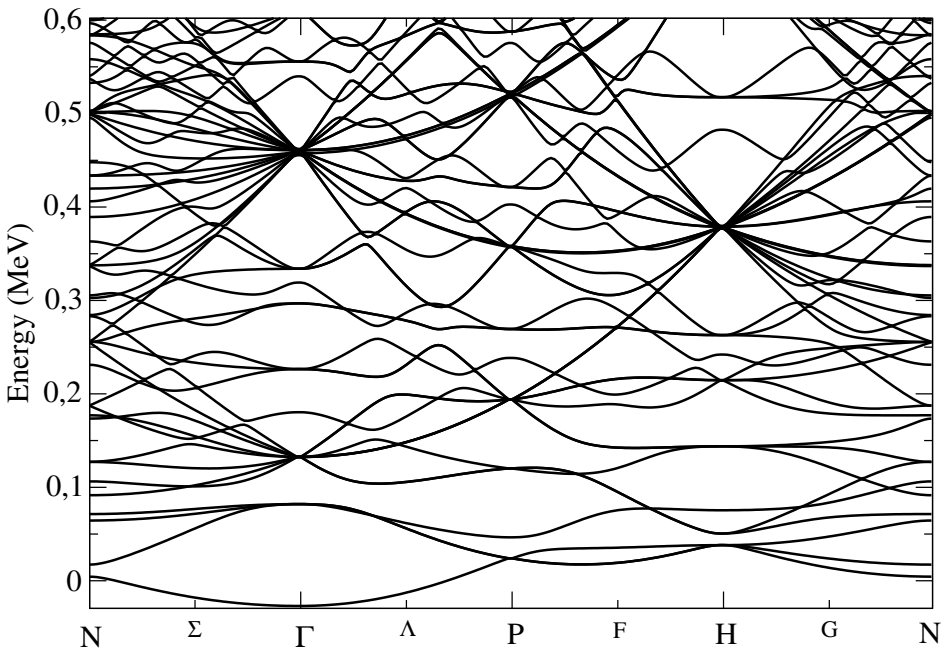

Chamel et al, Phys.Rev.C75, 055806 (2007)

"*Percolating network of linked nuclei*"

In 1982, Ogasawara and Sato speculated that **nuclei may globally connnect** by analogy with percolation networks:

3.3. *Formation of the percolating network of linked nuclei*

As pictured in Fig. 4, the ratio of the radius of a nucleus to the radius of the Wigner-Seitz cell increases as the density (and/or Y_L) increases. As a result nuclei begin to coalesce in the high density region. This occurs when the ratio R_N/R_C becomes $(8\pi/3)^{1/3}\sqrt{3}/4$ ($=0.88$) or $(4\pi)^{1/3}\sqrt{2}/4$ ($=0.82$) if the nuclei form the b.c.c. lattice, which is the most stable structure of the Coulomb crystal, or the f.c.c. lattice, respectively. If we neglect the Coulomb interaction among nuclei, the percolating network of linked nuclei may be formed when $R_N/R_C \approx (0.3)^{1/3}$ ($=0.67$) from the theories of percolations when the nuclei form no ordered structure and are randomly distributed.[26] Although the effect of the Coulomb repulsion among nuclei[27] could cause to change the critical value of percolation, it is plausible to

Ogasawara&Sato, Prog. Theor. Phys. 68, 222 (1982)

Nuclear "pastas": first predictions

Nuclear "pastas" were first studied based on liquid-drop models.

Ravenhall et al., PRL50, 2066 (1983);Hashimoto et al., PTP71, 320 (1984)

Oyamatsu et al., PTP 72, 373 (1984)

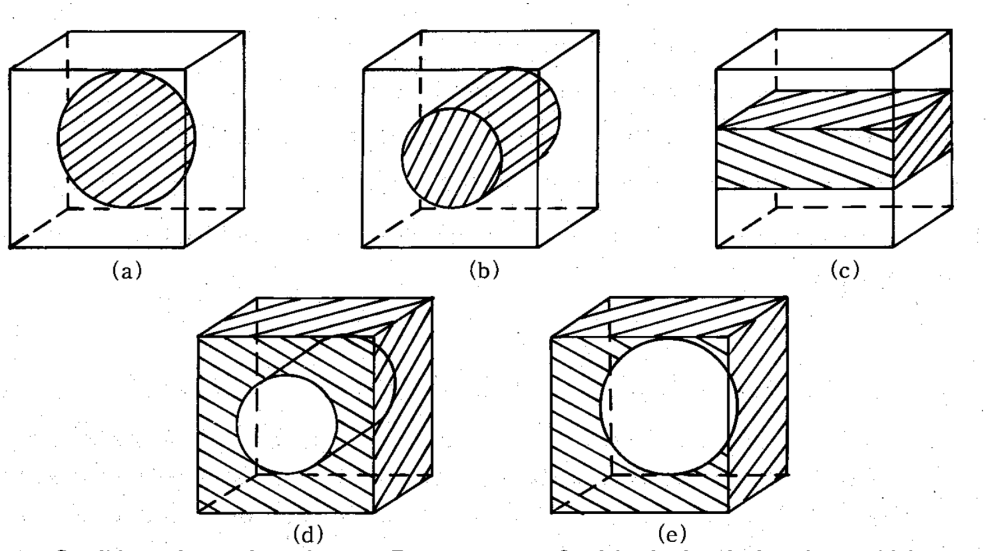

Gnocchi *Spaghetti* *Lasagna*

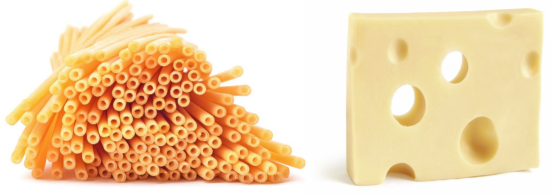

Bucatini *Swiss cheese*

Nuclear "pastas": first predictions

Nuclear "pastas" were first studied based on liquid-drop models.

Ravenhall et al., PRL50, 2066 (1983);Hashimoto et al., PTP71, 320 (1984)

Oyamatsu et al., PTP 72, 373 (1984)

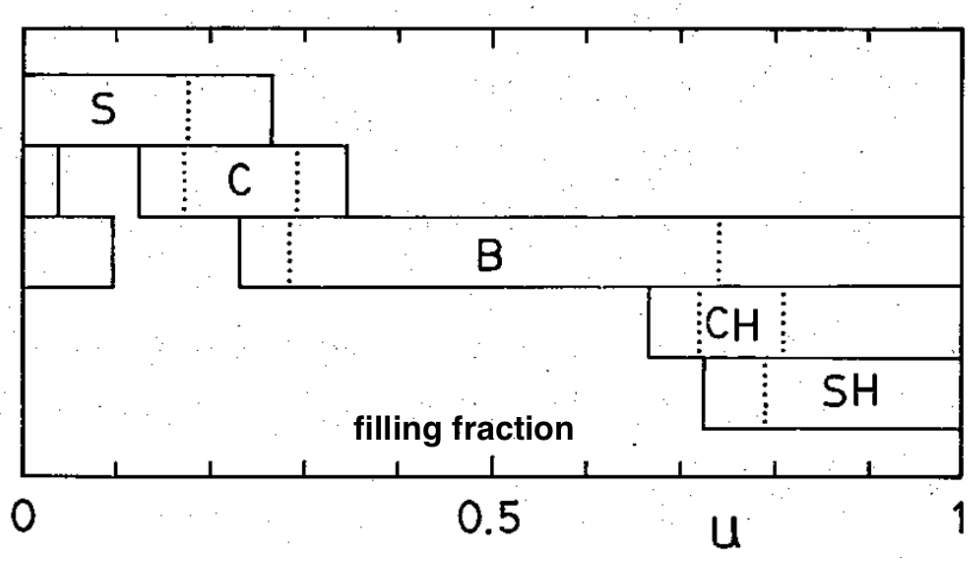

With increasing filling fraction ($u \gtrsim 0.2$): gnocchi (S), spaghetti (C), lasagna (B), bucatini (CH), and Swiss cheese (SH).

Nuclear "pastas": first predictions

Nuclear "pastas" were first studied based on liquid-drop models.

Ravenhall et al., PRL50, 2066 (1983);Hashimoto et al., PTP71, 320 (1984)

Oyamatsu et al., PTP 72, 373 (1984)

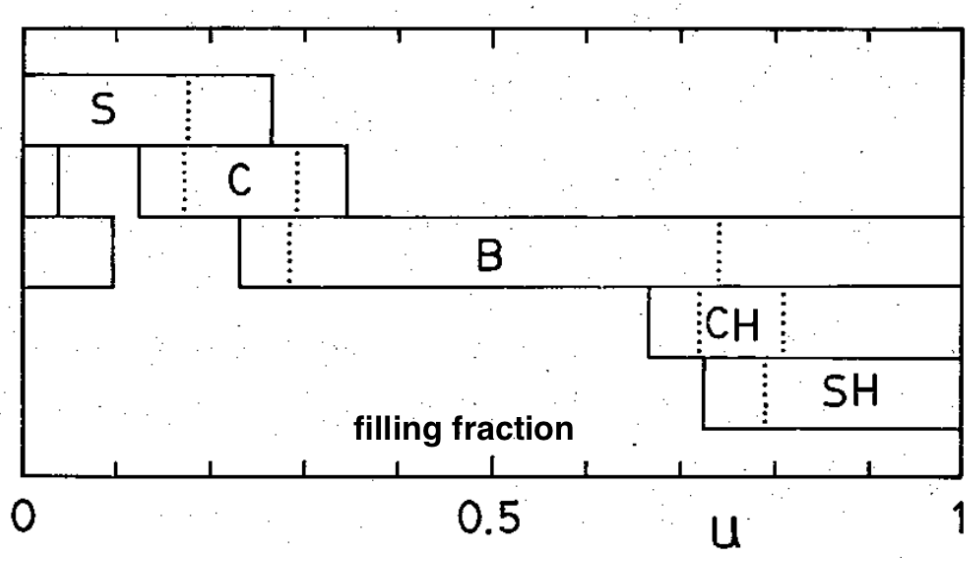

With increasing filling fraction ($u \gtrsim 0.2$): gnocchi (S), spaghetti (C), lasagna (B), bucatini (CH), and Swiss cheese (SH).

However, the existence of nuclear pastas can be altered by various corrections (e.g., neutron skin, curvature, etc).

Nuclear pastas in neutron stars

According to recent liquid-drop model calculations, pastas could represent about **50% of the mass of neutron-star crust**.

e.g. *Newton et al. EpJA58, 69 (2022); Dinh Thi et al., A&A 654, A114 (2021)*

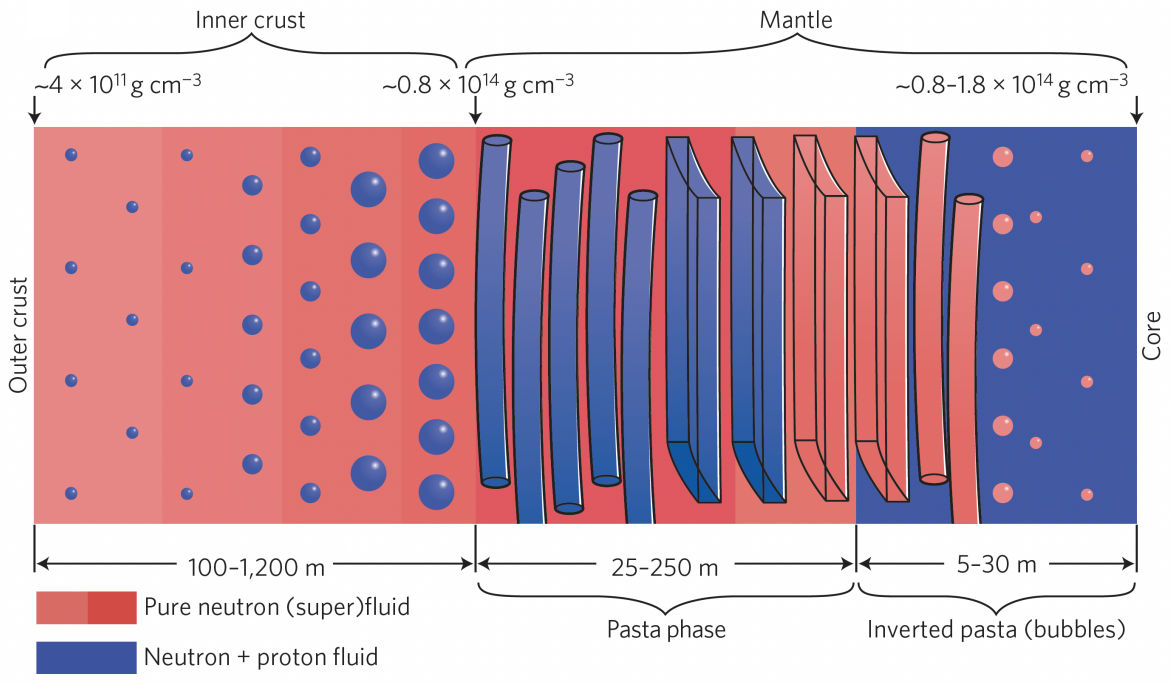

W. G. Newton, Nature Phys. 9, 396 (2013)

Pastas could have implications for thermal and dynamical evolutions of neutron stars and their magnetic field, gravitational-wave emission.

Quantum physics of nuclear pastas

To which extent do shell effects and nuclear pairing impact the existence of nuclear pastas?

Quantum physics of nuclear pastas

To which extent do shell effects and nuclear pairing impact the existence of nuclear pastas?

This question can be addressed using the **nuclear energy-density functional theory**: nucleons are treated as independent quasiparticles in self-consistent “mean” fields.

Quantum physics of nuclear pastas

To which extent do shell effects and nuclear pairing impact the existence of nuclear pastas?

In practice, one must solve the **Hartree-Fock-Bogoliubov** equations for both neutrons and protons ($q = n, p$):

$$\sum_{\sigma'} \begin{pmatrix} h'_q(\boldsymbol{r})_{\sigma\sigma'} & \Delta_q(\boldsymbol{r})\delta_{\sigma\sigma'} \\ \Delta_q(\boldsymbol{r})^*\delta_{\sigma\sigma'} & -\sigma\sigma' h'_q(\boldsymbol{r})^*_{-\sigma-\sigma'} \end{pmatrix} \begin{pmatrix} \psi_1^{(q)}(\boldsymbol{r},\sigma') \\ \psi_2^{(q)}(\boldsymbol{r},\sigma') \end{pmatrix} = \mathfrak{E}^{(q)} \begin{pmatrix} \psi_1^{(q)}(\boldsymbol{r},\sigma) \\ \psi_2^{(q)}(\boldsymbol{r},\sigma) \end{pmatrix}$$

These equations are similar to the **Bogoliubov-de Gennes equations** but the Hamiltonian $h'_q(\boldsymbol{r})_{\sigma\sigma'}$ is more complicated

Quantum physics of nuclear pastas

To which extent do shell effects and nuclear pairing impact the existence of nuclear pastas?

In practice, one must solve the **Hartree-Fock-Bogoliubov** equations for both neutrons and protons ($q = n, p$):

$$\sum_{\sigma'} \begin{pmatrix} h'_q(\boldsymbol{r})_{\sigma\sigma'} & \Delta_q(\boldsymbol{r})\delta_{\sigma\sigma'} \\ \Delta_q(\boldsymbol{r})^*\delta_{\sigma\sigma'} & -\sigma\sigma' h'_q(\boldsymbol{r})^*_{-\sigma-\sigma'} \end{pmatrix} \begin{pmatrix} \psi_1^{(q)}(\boldsymbol{r},\sigma') \\ \psi_2^{(q)}(\boldsymbol{r},\sigma') \end{pmatrix} = \mathfrak{E}^{(q)} \begin{pmatrix} \psi_1^{(q)}(\boldsymbol{r},\sigma) \\ \psi_2^{(q)}(\boldsymbol{r},\sigma) \end{pmatrix}$$

$$h'_q(\boldsymbol{r})_{\sigma'\sigma} \equiv \left[-\boldsymbol{\nabla}\cdot\frac{\delta E}{\delta\tau_q(\boldsymbol{r})}\boldsymbol{\nabla} + \frac{\delta E}{\delta n_q(\boldsymbol{r})} - \lambda_q \right]\delta_{\sigma\sigma'} - \mathrm{i}\frac{\delta E}{\delta \boldsymbol{J_q}(\boldsymbol{r})}\cdot\boldsymbol{\nabla}\times\hat{\boldsymbol{\sigma}}_{\sigma'\sigma} + \ldots$$

$\Delta_q(\boldsymbol{r}) = 2\dfrac{\delta E}{\delta\widetilde{n}_q(\boldsymbol{r})^*}$ is the potential responsible for nucleon pairing

$n_q(\boldsymbol{r})$, $\tau_q(\boldsymbol{r})$, $\boldsymbol{J_q}(\boldsymbol{r})\ldots$ are defined from the density matrices

$$n_q(\boldsymbol{r},\sigma;\boldsymbol{r'},\sigma') = \langle\Psi|c_q(\boldsymbol{r'},\sigma')^\dagger c_q(\boldsymbol{r},\sigma)|\Psi\rangle$$
$$\widetilde{n}_q(\boldsymbol{r},\sigma;\boldsymbol{r'},\sigma') = -\sigma'\langle\Psi|c_q(\boldsymbol{r'},-\sigma')c_q(\boldsymbol{r},\sigma)|\Psi\rangle,$$

which in turn depend on $\psi_1^{(q)}(\boldsymbol{r},\sigma)$ and $\psi_2^{(q)}(\boldsymbol{r},\sigma)$.

Quantum physics of nuclear pastas

The HFB equations are highly nonlinear and computationally challenging to solve in 3D in the pasta region ($N \sim 10^3$).

Quantum physics of nuclear pastas

The HFB equations are highly nonlinear and computationally challenging to solve in 3D in the pasta region ($N \sim 10^3$).

Extended Thomas-Fermi+Strutinsky Integral (ETFSI) approach:

- **semiclassical expansion in powers of** $\hbar$: the energy E becomes a functional of $n_q(\boldsymbol{r})$ and their derivatives only.
- **shell effects and pairing** are added perturbatively and consistently via the SI theorem.
- allowance for different (fixed) pasta shapes,
- to speed-up the computations, $n_q(\boldsymbol{r})$ are parametrized.

Pearson&Chamel, Phys.Rev.C105,015803(2022); *Phys.Rev.C101,015802(2020)*

The ETFSI method is a fairly accurate and computationally very fast approximation to the HFB equations

Shelley&Pastore, Universe 6, 206 (2020)

Brussels Skyrme functionals BSk(G)

We have fitted a series of nuclear energy-density functionals with full HFB calculations based on extended Skyrme effective interactions

Experimental data/constraints:

- $\sim$ 2300 atomic masses (rms $\sim 0.5 - 0.6$ MeV$/c^2$)
- $\sim$ 900 nuclear charge radii (rms $\sim$ 0.03 fm)
- symmetry energy $29 \leq J \leq 32$ MeV
- incompressibility $K_v = 240 \pm 10$ MeV (giant resonances in nuclei)

Many-body ab initio calculations:

- equation of state of pure neutron matter
- $^1S_0$ pairing gaps in nuclear matter
- effective masses in nuclear matter (+giant resonances in nuclei)
- stability against spin and spin-isospin fluctuations

Grams et al., Eur. Phys. J. A 59, 270 (2023)

BSk22-26 family

BSk22-26 were adjusted to different values of $J = S(n_0)$. The fit to nuclear masses actually fixes $S(n)$ around $n \sim 0.1$ fm^{-3}:

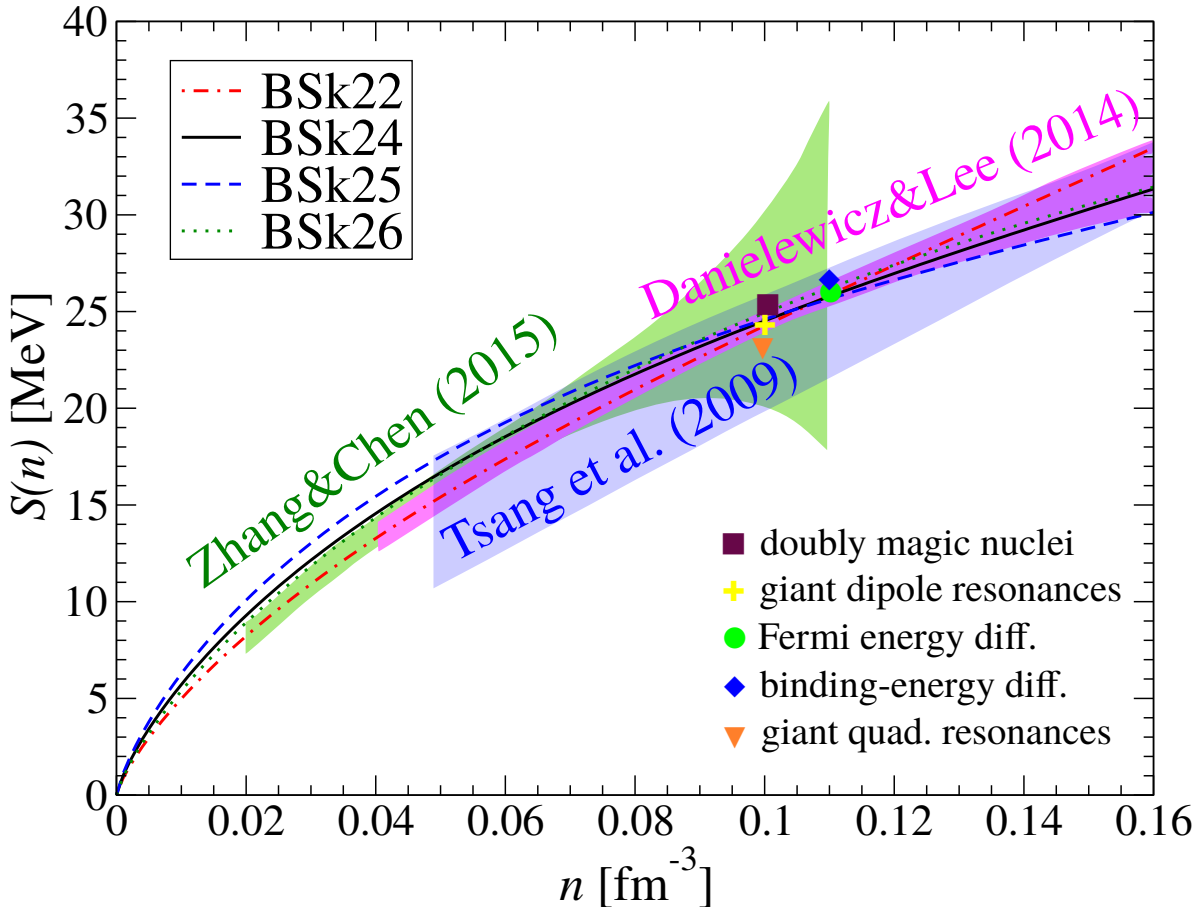

Goriely, Chamel, Pearson, Phys.Rev.C 88, 024308 (2013)

Nuclear-matter parameters

	BSk22	BSk23	BSk24	BSk25	BSk26
a_v [MeV]	-16.088	-16.068	-16.048	-16.032	-16.064
n_0 [fm^{-3}]	0.1578	0.1578	0.1578	0.1587	0.1589
J [MeV]	32.0	31.0	30.0	29.0	30.0
L [MeV]	68.5	57.8	46.4	36.9	37.5
K_{sym}[MeV]	13.0	-11.3	-37.6	-28.5	-135.6
K_v [MeV]	245.9	245.7	245.5	236.0	240.8
K' [MeV]	275.5	275.0	274.5	316.5	282.9
M_s^*/M	0.80	0.80	0.80	0.80	0.80
M_v^*/M	0.71	0.71	0.71	0.74	0.65
NeuM	BHF	BHF	BHF	BHF	APR

Lower and higher values of J were considered but yielded substantially worse fits to atomic masses.

BHF: 'V18' from *Li & Schulze, PRC 78, 028801 (2008)*
APR: 'A18 + δv + UIX*' from *Akmal et al., PRC 58, 1804 (1998)*

Neutron-matter constraint

BSk22-26 are in reasonably good agreement with more recent neutron-matter calculations based on chiral effective-field theory:

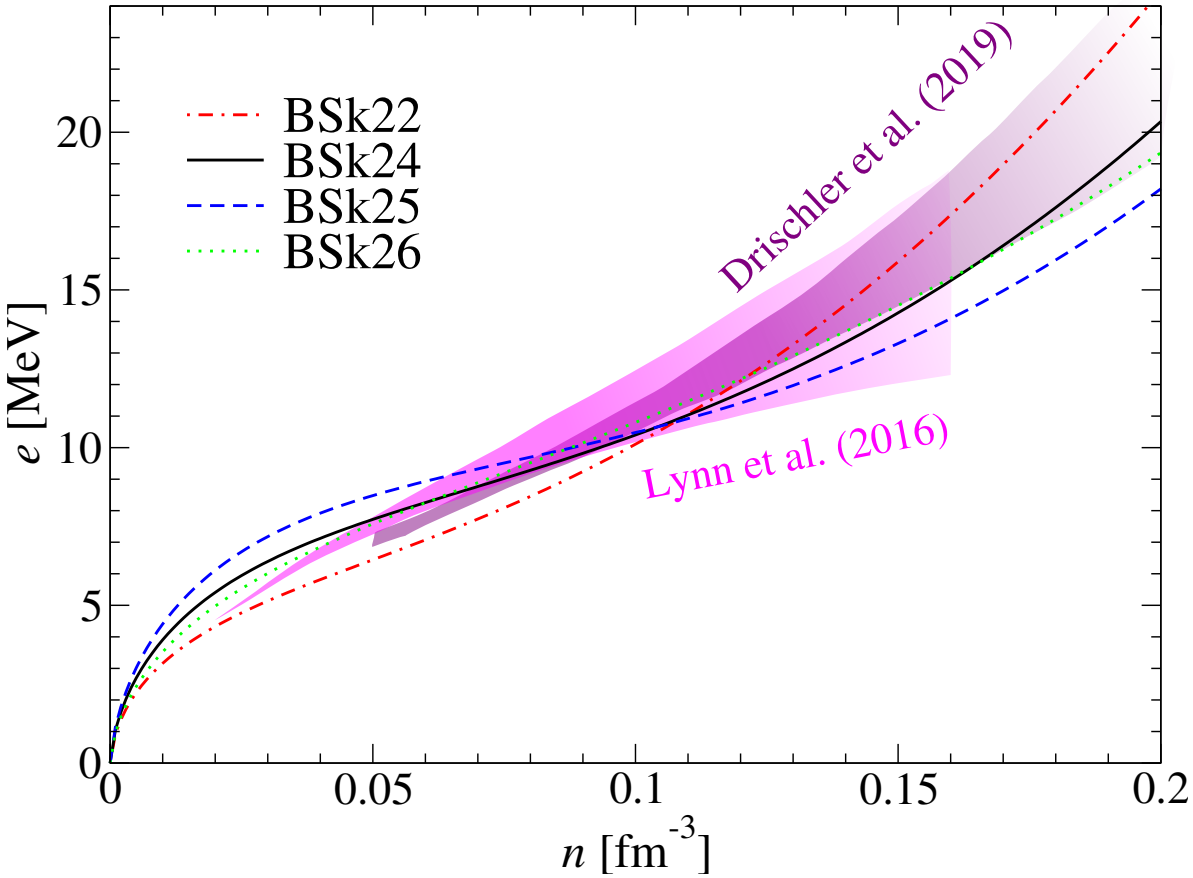

Lynn et al. (2016) calculations at N2LO
Drischler et al. (2019) calculations at N3LO

Nuclear pastas with ETF(SI) approach

Ignoring SI correction (pure ETF calculations):

- Similar pasta sequence as liquid-drop models
- Negligible impact ($< 1\%$) on the equation of state

Pearson, Chamel, Potekhin, Phys. Rev. C 101, 015802 (2020)

Nuclear pastas with ETF(SI) approach

Ignoring SI correction (pure ETF calculations):

- Similar pasta sequence as liquid-drop models
- Negligible impact ($< 1\%$) on the equation of state

Pearson, Chamel, Potekhin, Phys. Rev. C 101, 015802 (2020)

With SI correction, spaghetti are strongly disfavored!

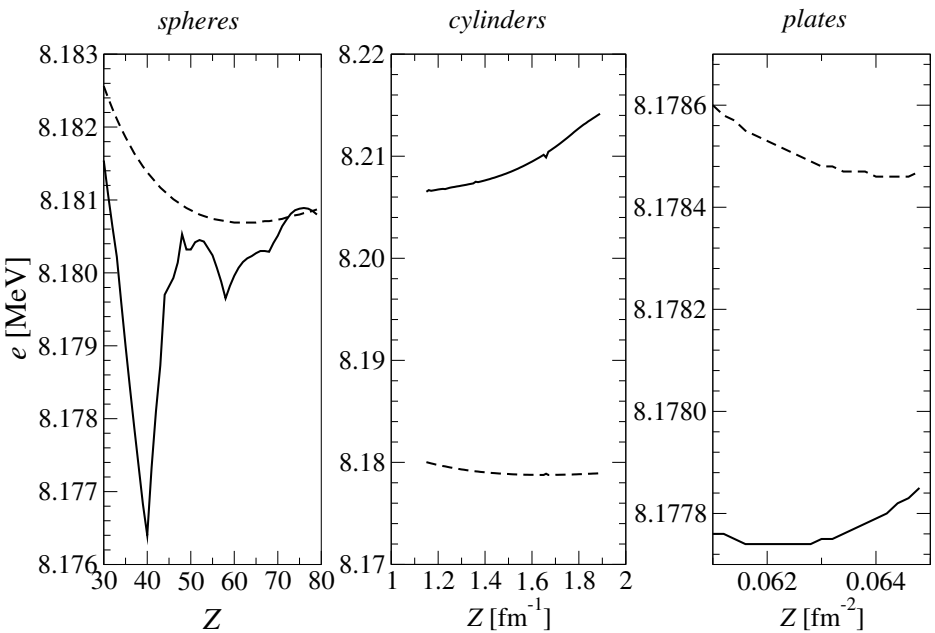

- No true “shell” effects in pastas (smooth fluctuations)
- Origin of SI correction: overbinding of ETF vs HFB, underbinding due to parametrized nucleon profiles

Pearson&Chamel, Phys. Rev. C 105, 015803 (2022)

Quantum structure of pastas

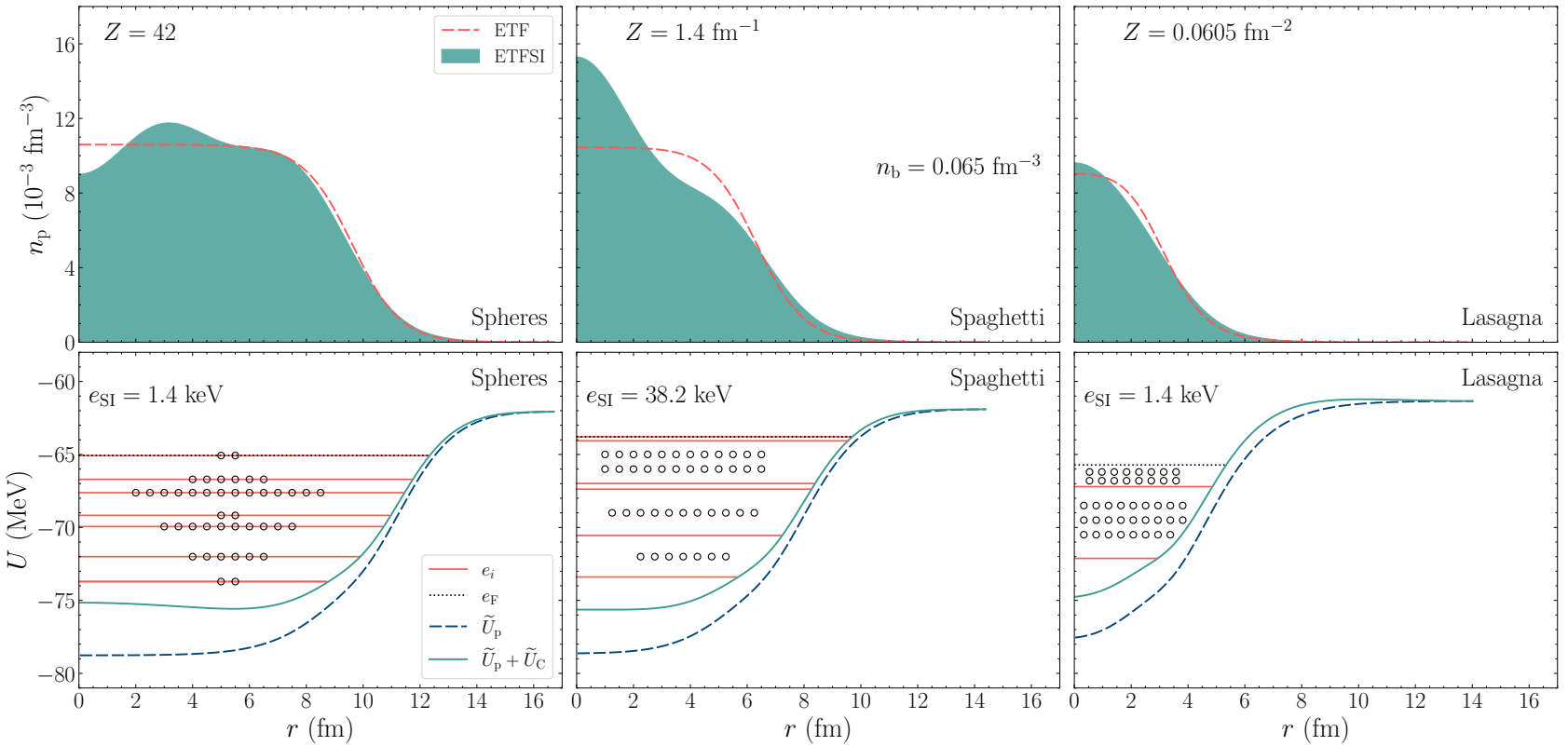

Two competing effects:

- The narrower potential for spaghetti and lasagna tends to shift the energy levels to higher values than for spheres.
- More nucleons can fill in the interlevel spacing for lasagna than for spaghetti.

Shchechilin et al., Phys. Rev. C in press

Nuclear pastas and symmetry energy - ETF

Pasta phases are more likely to appear for models with higher values of the symmetry energy at the relevant densities (BSk22 vs BSk25):

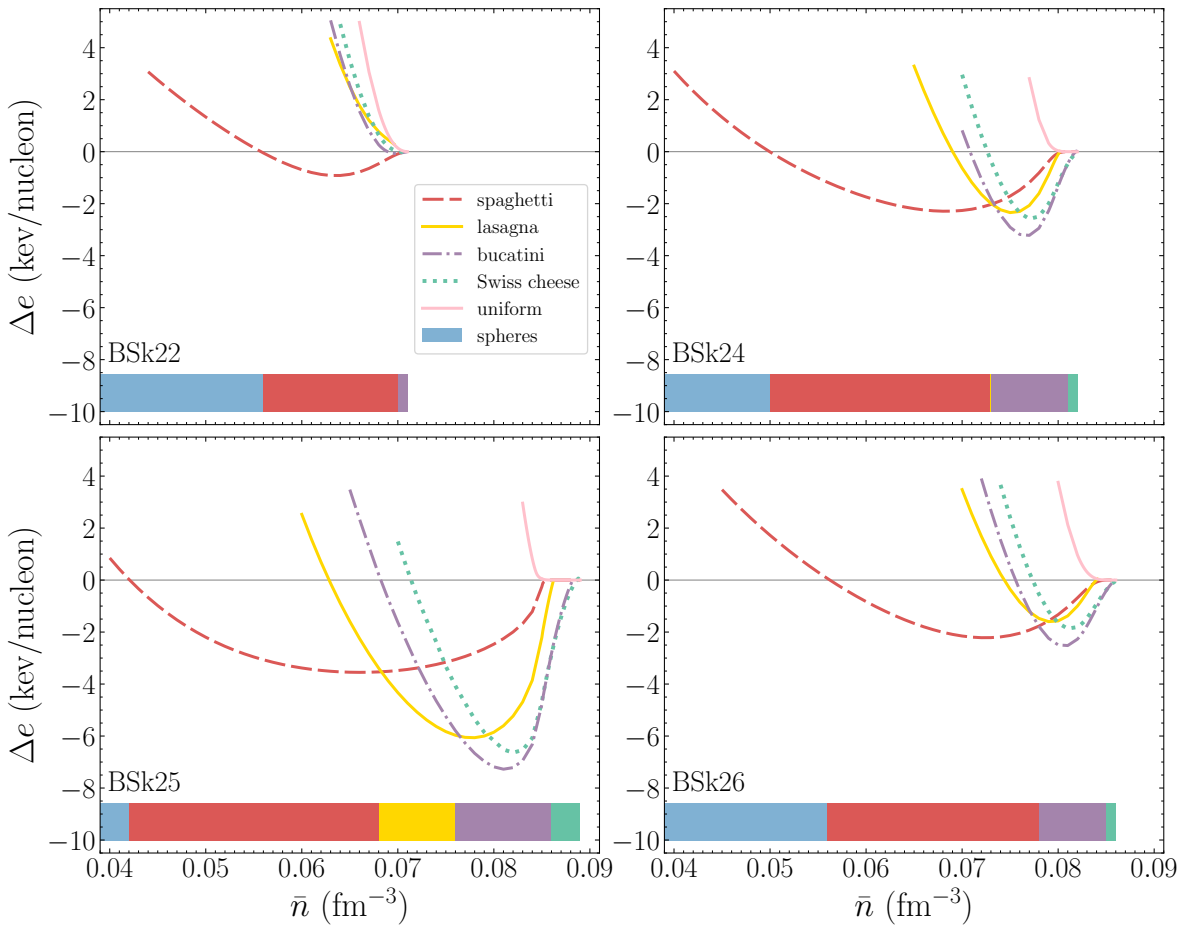

Shchechilin, Chamel, Pearson, Phys. Rev. C108, 025805 (2023)

Nuclear pastas and symmetry energy - ETFSI

Pasta phases occupy a much narrower range of densities, and correlations with symmetry energy vanish:

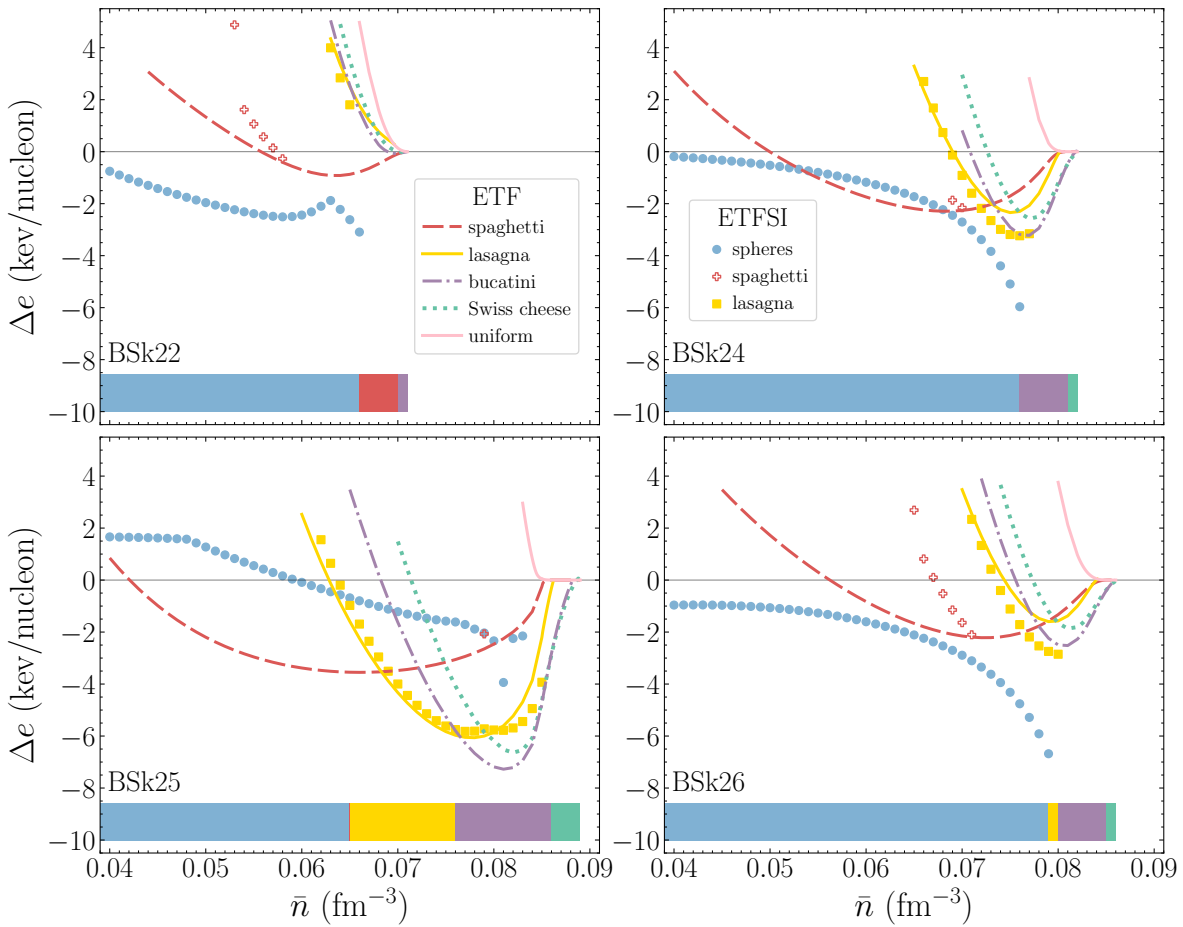

Shchechilin, Chamel, Pearson, Phys. Rev. C108, 025805 (2023)

Nuclear pastas abundances in neutron stars

The pasta mantle shrinks dramatically with shell effects!

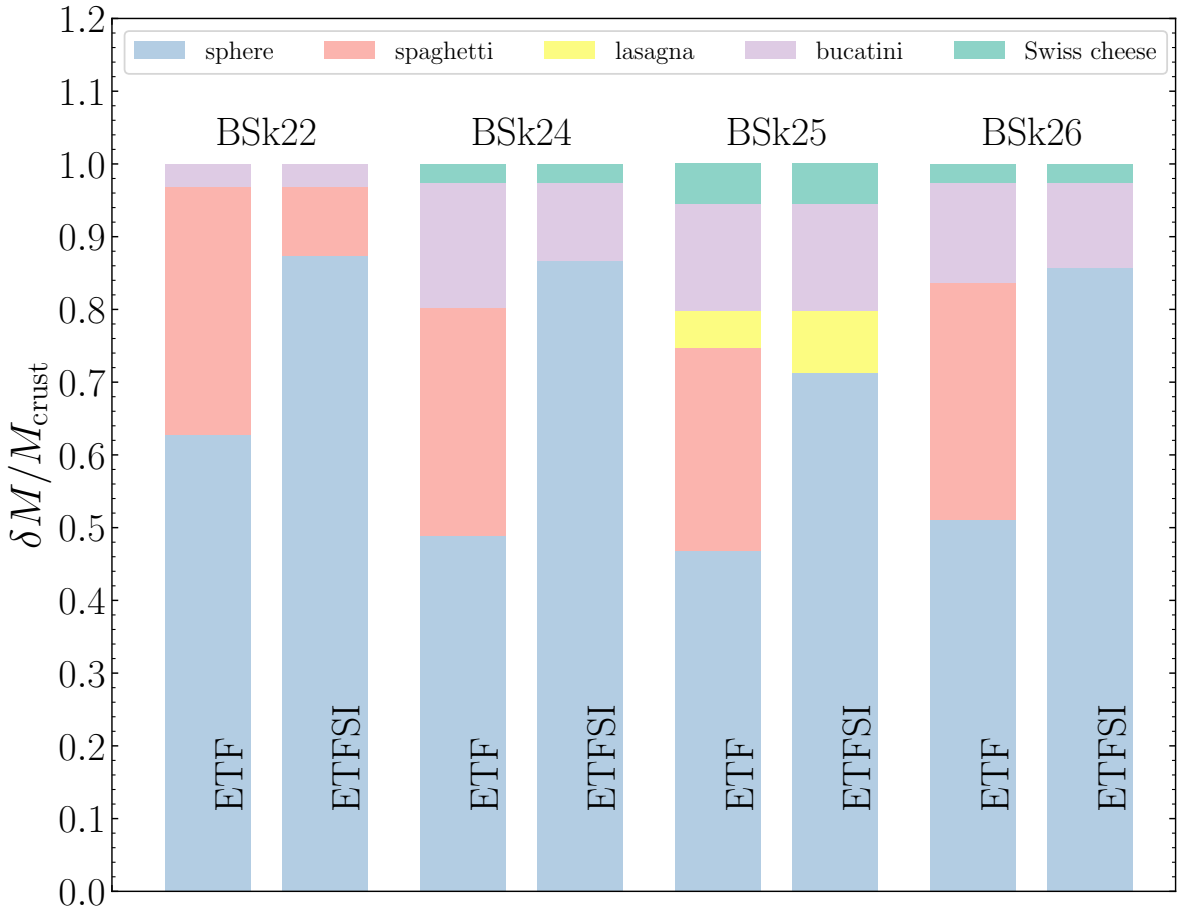

Shchechilin, Chamel, Pearson, Phys. Rev. C108, 025805 (2023)

Role of the nucleon density parametrization

At very high densities, results are sensitive to the choice of the parametrization of $n_q(\xi)$ in the Wigner-Seitz cell of "radius" R.

Writing the nucleon density as $n_q(\xi) = n_{\mathrm{B}q} + n_{\Lambda q} f_q(\xi)$,

the popular ansatz ($n_{\mathrm{B}q}$, $n_{\Lambda q}$, C_q, a_q are free parameters)

$$f_q^{\mathrm{FD}}(\xi) = \frac{1}{1 + \exp\left(\frac{\xi - C_q}{a_q}\right)}$$

does not satisfy the boundary condition $\dfrac{dn_q}{d\xi}(\xi = R) = 0$.

Role of the nucleon density parametrization

At very high densities, results are sensitive to the choice of the parametrization of $n_q(\xi)$ in the Wigner-Seitz cell of "radius" R.

Writing the nucleon density as $n_q(\xi) = n_{\mathrm{B}q} + n_{\Lambda q} f_q(\xi)$,

the ansatz we adopted since 2008

$$f_q^{\mathrm{StrD}}(\xi) = \frac{1}{1 + \exp\left[\left(\frac{C_q - R}{\xi - R}\right)^2 - 1\right] \exp\left(\frac{\xi - C_q}{a_q}\right)}$$

does satisfy $\frac{dn_q}{d\xi}(\xi = R) = 0$ but all derivatives actually vanish.

Onsi et al., Phys.Rev.C77,065805 (2008)

Role of the nucleon density parametrization

At very high densities, results are sensitive to the choice of the parametrization of $n_q(\xi)$ in the Wigner-Seitz cell of "radius" R.

Writing the nucleon density as $n_q(\xi) = n_{\mathrm{B}q} + n_{\Lambda q} f_q(\xi)$,

our new ansatz is

$$f_q^{\mathrm{SoftD}}(\xi) = \frac{1}{1 + \left(\frac{C_q - R}{C_q}\right)^2 \left(\frac{\xi}{\xi - R}\right)^2 \exp\left(\frac{\xi - C_q}{a_q}\right)}$$

satisfies $\dfrac{dn_q}{d\xi}(\xi = 0) = \dfrac{dn_q}{d\xi}(\xi = R) = 0.$

We also consider

$$f_q^{3\mathrm{FD}}(\xi) = f_q^{\mathrm{FD}}(-\xi) + f_q^{\mathrm{FD}}(\xi) + f_q^{\mathrm{FD}}(2R - \xi) - f_q^{\mathrm{FD}}(-R) - 2f_q^{\mathrm{FD}}(R)$$

Role of the nucleon density parametrization

- All parametrizations agree up to the point where pastas first appear at $\bar{n} \approx 0.07$ fm^{-3}.
- The two new parametrizations yield more stable configurations (lower energies).
- Both predict lasagna interspersed among gnocchis.

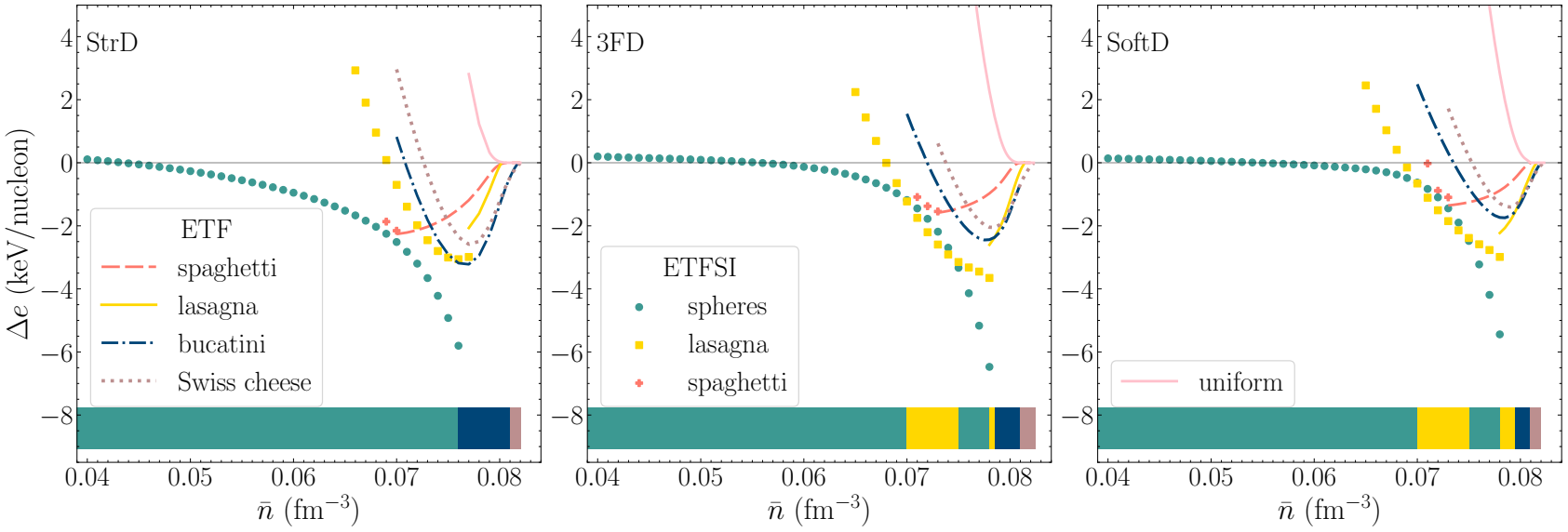

Shchechilin, Chamel, Pearson et al., Phys. Rev. C in press

Neutron superfluidity in neutron-star crusts

Superstars

The huge gravity of neutron stars produces the highest-T_c and largest superfluids and superconductors known in the Universe!

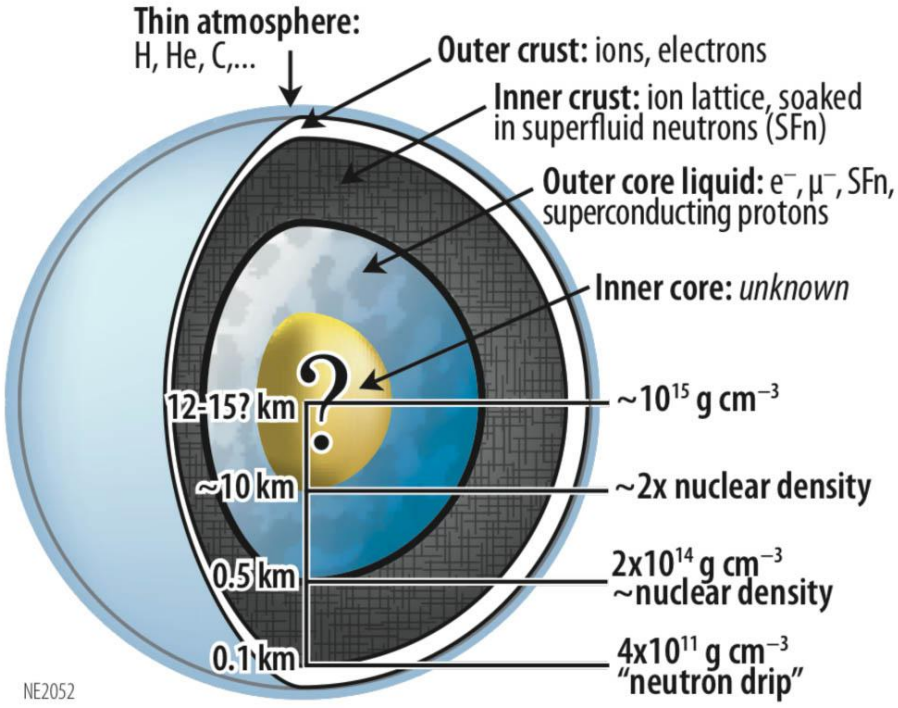

Neutron stars	**$\sim 10^{10}$ K**
⋮	⋮
$LaH_{10\pm x}$	260 K
Cuprates	$1 - 130$ K
Electrons in metals	$1 - 25$ K
Helium-4	2.17 K
Helium-3	2.491×10^{-3} K
Bosonic condensates	$\sim 10^{-6}$ K
Fermionic condensates	$\sim 10^{-8}$ K

Predicted long ago, these quantum phases may be probed through astrophysical observations.

Pulsar frequency glitches and superfluidity

Pulsars are spinning very rapidly with **extremely stable periods** $\dot{P} \gtrsim 10^{-21}$, outperforming the best atomic clocks!

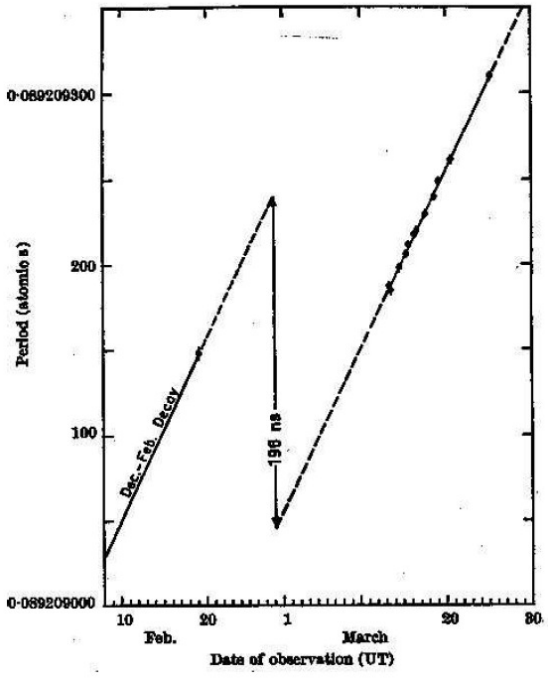

Still, some pulsars have been found to **suddenly spin up** (in less than a minute).

672 glitches have been detected in 225 pulsars.

`http://www.jb.man.ac.uk/pulsar/glitches.html`

Recent review: *Antonopoulou, Haskell, Espinoza, Rep. Prog. Phys. 85, 126901 (2022)*

Experimental glitches with ultracold atoms

Poli et al., PRL 131, 223401 (2023)

Pulsar glitches provide strong evidence for the existence of a **neutron superflow in neutron-star crusts** driven by the pinning of quantized vortices. But the superfluid dynamics remains poorly understood.

Time-dependent Hartree-Fock-Bogoliubov theory

The dynamics of nuclear superfluids ($q = n, p$) is here described by the **time-dependent Hartree-Fock-Bogoliubov equations**:

$$\begin{pmatrix} h_q(\boldsymbol{r},t) - \lambda_q & \Delta_q(\boldsymbol{r},t) \\ \Delta_q(\boldsymbol{r},t)^* & -h_q(\boldsymbol{r},t)^* + \lambda_q \end{pmatrix} \begin{pmatrix} \psi_1^{(q)}(\boldsymbol{r},t) \\ \psi_2^{(q)}(\boldsymbol{r},t) \end{pmatrix} = \mathrm{i}\hbar \frac{\partial}{\partial t} \begin{pmatrix} \psi_1^{(q)}(\boldsymbol{r},t) \\ \psi_2^{(q)}(\boldsymbol{r},t) \end{pmatrix}$$

Time-dependent Hartree-Fock-Bogoliubov theory

The dynamics of nuclear superfluids ($q = n, p$) is here described by the **time-dependent Hartree-Fock-Bogoliubov equations**:

$$\begin{pmatrix} h_q(\boldsymbol{r},t) - \lambda_q & \Delta_q(\boldsymbol{r},t) \\ \Delta_q(\boldsymbol{r},t)^* & -h_q(\boldsymbol{r},t)^* + \lambda_q \end{pmatrix} \begin{pmatrix} \psi_1^{(q)}(\boldsymbol{r},t) \\ \psi_2^{(q)}(\boldsymbol{r},t) \end{pmatrix} = \mathrm{i}\hbar \frac{\partial}{\partial t} \begin{pmatrix} \psi_1^{(q)}(\boldsymbol{r},t) \\ \psi_2^{(q)}(\boldsymbol{r},t) \end{pmatrix}$$

These equations are similar to the **Bogoliubov-de Gennes equations**, but the Hamilonian takes a more complicated form

Time-dependent Hartree-Fock-Bogoliubov theory

The dynamics of nuclear superfluids ($q = n, p$) is here described by the **time-dependent Hartree-Fock-Bogoliubov equations**:

$$\begin{pmatrix} h_q(\boldsymbol{r},t) - \lambda_q & \Delta_q(\boldsymbol{r},t) \\ \Delta_q(\boldsymbol{r},t)^* & -h_q(\boldsymbol{r},t)^* + \lambda_q \end{pmatrix} \begin{pmatrix} \psi_1^{(q)}(\boldsymbol{r},t) \\ \psi_2^{(q)}(\boldsymbol{r},t) \end{pmatrix} = \mathrm{i}\hbar \frac{\partial}{\partial t} \begin{pmatrix} \psi_1^{(q)}(\boldsymbol{r},t) \\ \psi_2^{(q)}(\boldsymbol{r},t) \end{pmatrix}$$

$$h_q(\boldsymbol{r},t) \equiv -\boldsymbol{\nabla} \cdot \frac{\hbar^2}{2m_q^{\oplus}(\boldsymbol{r},t)} \boldsymbol{\nabla} + U_q(\boldsymbol{r},t) - \frac{\mathrm{i}}{2} \{ \boldsymbol{I_q}(\boldsymbol{r},t), \boldsymbol{\nabla} \} + \ldots$$

$$\frac{\hbar^2}{2m_q^{\oplus}(\boldsymbol{r},t)} = \frac{\delta E}{\delta \tau_q(\boldsymbol{r},t)}, \quad U_q(\boldsymbol{r},t) = \frac{\delta E}{\delta n_q(\boldsymbol{r},t)}, \quad \boldsymbol{I_q}(\boldsymbol{r},t) = \frac{\delta E}{\delta \boldsymbol{j_q}(\boldsymbol{r},t)}$$

$$\Delta_q(\boldsymbol{r},t) = 2 \frac{\delta E}{\delta \widetilde{n_q}(\boldsymbol{r},t)^*} = |\Delta_q(\boldsymbol{r},t)| e^{\mathrm{i}\phi_q(\boldsymbol{r},t)}$$

with mean fields defined via the particle and pair density matrices (thermal averages) expressible in terms of $\psi_1^{(q)}(\boldsymbol{r},t)$ and $\psi_2^{(q)}(\boldsymbol{r},t)$

$$n_q(\boldsymbol{r},\sigma;\boldsymbol{r}',\sigma';t) = < c_q(\boldsymbol{r}',\sigma';t)^\dagger c_q(\boldsymbol{r},\sigma;t) >$$

$$\widetilde{n}_q(\boldsymbol{r},\sigma;\boldsymbol{r}',\sigma';t) = -\sigma' < c_q(\boldsymbol{r}',-\sigma';t) c_q(\boldsymbol{r},\sigma;t) >$$

Superfluid velocity, momentum and mass transport

The **superfluid velocity** defined through the phase of the pairing field

$$\Delta_q(\boldsymbol{r},t) = |\Delta_q(\boldsymbol{r},t)|e^{\mathrm{i}\phi_q(\boldsymbol{r},t)} \qquad \Rightarrow \boldsymbol{V_q}(\boldsymbol{r},t) = \frac{\hbar}{2m_q}\boldsymbol{\nabla}\phi_q(\boldsymbol{r},t)$$

Superfluid velocity, momentum and mass transport

The **superfluid velocity** defined through the phase of the pairing field

$$\Delta_q(\boldsymbol{r},t) = |\Delta_q(\boldsymbol{r},t)|e^{\mathrm{i}\phi_q(\boldsymbol{r},t)} \qquad \Rightarrow \boldsymbol{V_q}(\boldsymbol{r},t) = \frac{\hbar}{2m_q}\nabla\phi_q(\boldsymbol{r},t)$$

is neither equal to $\hbar\boldsymbol{j_q}/\rho_q$ where $\boldsymbol{j_q}$ is the **momentum density**

$$\boldsymbol{j_q}(\boldsymbol{r},t) = -\frac{i}{2}\sum_{\sigma=\pm1}\int \mathrm{d}^3\boldsymbol{r'}\,\delta(\boldsymbol{r}-\boldsymbol{r'})(\nabla-\nabla')n_q(\boldsymbol{r},\sigma;\boldsymbol{r'},\sigma;t)$$

Superfluid velocity, momentum and mass transport

The **superfluid velocity** defined through the phase of the pairing field

$$\Delta_q(\boldsymbol{r},t) = |\Delta_q(\boldsymbol{r},t)|e^{\mathrm{i}\phi_q(\boldsymbol{r},t)} \qquad \Rightarrow \boldsymbol{V_q}(\boldsymbol{r},t) = \frac{\hbar}{2m_q}\boldsymbol{\nabla}\phi_q(\boldsymbol{r},t)$$

is neither equal to $\hbar\boldsymbol{j_q}/\rho_q$ where $\boldsymbol{j_q}$ is the **momentum density**

$$\boldsymbol{j_q}(\boldsymbol{r},t) = -\frac{i}{2}\sum_{\sigma=\pm1}\int \mathrm{d}^3\boldsymbol{r'}\,\delta(\boldsymbol{r}-\boldsymbol{r'})(\boldsymbol{\nabla}-\boldsymbol{\nabla'})n_q(\boldsymbol{r},\sigma;\boldsymbol{r'},\sigma;t)$$

nor to the velocity

$$\boldsymbol{v_q}(\boldsymbol{r},t) = \frac{m_q}{m_q^{\oplus}(\boldsymbol{r},t)}\frac{\hbar\boldsymbol{j_q}(\boldsymbol{r},t)}{\rho_q(\boldsymbol{r},t)} + \frac{\boldsymbol{I_q}(\boldsymbol{r},t)}{\hbar}$$

associated with **mass transport**

$$\frac{\partial\rho_q}{\partial t} + \boldsymbol{\nabla}\cdot(\rho_q\boldsymbol{v_q}) = 0$$

Chamel & Allard, PRC100, 065801 (2019); *Allard & Chamel, PRC103, 025804 (2021)*

Neutron superfluidity in neutron-star crusts

The **breaking of translational symmetry** leads to the depletion of the superfluid reservoir.

Leggett, PRL 25, 1543 (1970)

In the presence of a **superflow** with velocity $\boldsymbol{V_n}$, the average neutron mass current in the rest frame of the neutron-star crust is

$$\bar{\rho}_n^i \equiv \frac{1}{V}\int \mathrm{d}^3 r\, \rho_n(\boldsymbol{r},t) v_n^i(\boldsymbol{r},t) = \sum_j \rho_s^{ij} \bar{V}_{nj}$$

Treating the crust as a polycrystal $\bar{\boldsymbol{\rho}}_{\boldsymbol{n}} = \rho_{\mathrm{S}} \bar{\boldsymbol{V}}_{\boldsymbol{n}} = \rho_n \dfrac{m_n}{m_n^\star} \bar{\boldsymbol{V}}_{\boldsymbol{n}}$.

The superfluid density $\rho_{\mathrm{S}} < \rho_n$ ($m_n^\star > m_n$) is a **current-current response function**.

This "*is a derived concept and is not the density of anything*".

Feynman, Statistical Mechanics: A Set of Lectures.

Review: *Chamel, J. Low Temp. Phys. 189, 328 (2017)*

Band structure and Fermi surface

Bragg scattering leads to strong distortions of the Fermi surface.

Avoided band crossings where

$$|\nabla_{\boldsymbol{k}} \varepsilon_{\alpha \boldsymbol{k}}| \approx 0$$

translate into necks and holes reducing the Fermi surface area.

Both effects suppress the superfluid density.

In the limit of small currents and weak coupling $\Delta_{\alpha \boldsymbol{k}}/\varepsilon_{\mathrm{F}} \to 0$:

$$\rho_{\mathrm{S}} \approx \frac{m_n^2}{12\pi^3\hbar^2} \sum_{\alpha} \int_{\mathrm{F}} |\nabla_{\boldsymbol{k}} \varepsilon_{\alpha \boldsymbol{k}}| \mathrm{d}\mathcal{S}^{(\alpha)}$$

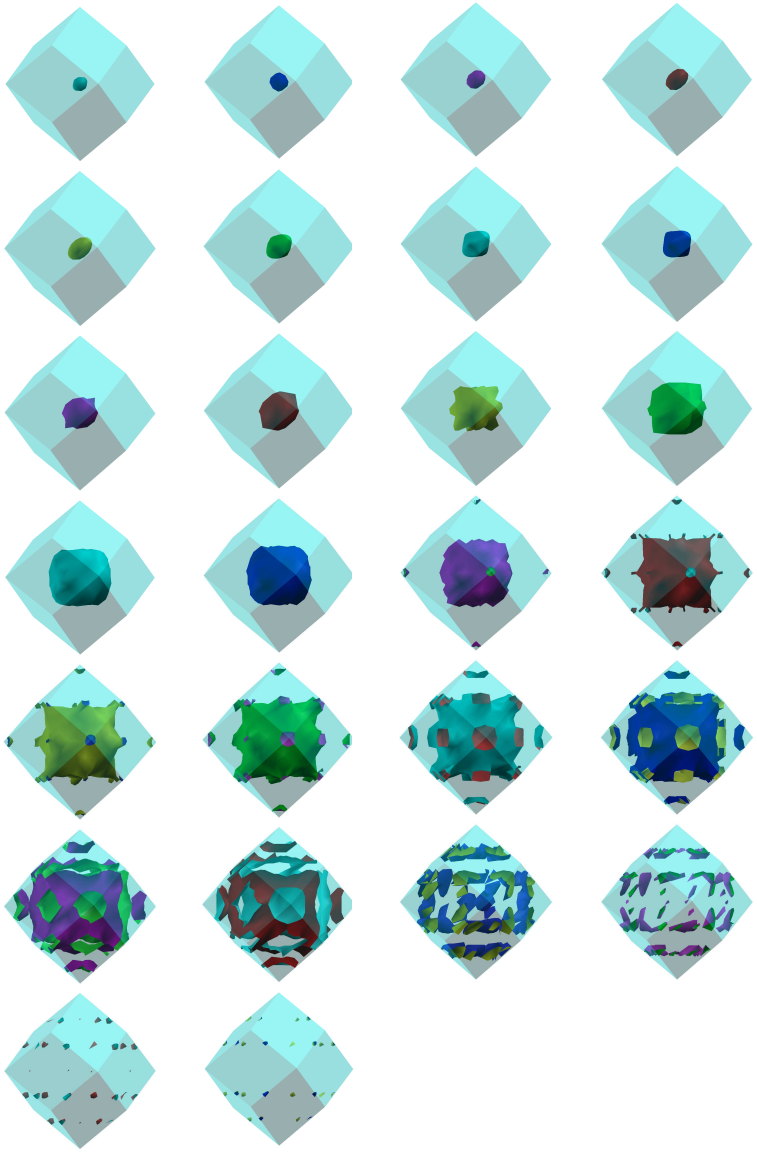

Picture made with XCrySDen

Neutron superfluid density from 3D band structure

Results of **full 3D band-structure calculations with BCS pairing** in the limit of small currents:

Δ (MeV)	$\Delta/\varepsilon_{\rm F}$	$\rho_{\rm S}/\rho_n$ (%)
1.59	0.0869	7.50
1.11	0.0604	7.50
0.770	0.0420	7.51
0.535	0.0292	7.54
0.372	0.0203	7.60
0.259	0.0141	7.66
0.180	0.00981	7.71
0.125	0.00682	7.76
0.0869	0.00474	7.80
0.0604	0.00330	7.82
0.0420	0.00229	7.84

baryon density $\bar{n} = 0.03$ fm^{-3}
bcc lattice spacing 47.3 fm
1550 neutrons in the Wigner-Seitz cell

$25 \times 25 \times 25$ points ($\delta r \sim 0.95$ fm)
$\sim$ 1300 bands (half without pairing)

integrations with 1360 special ***k*** points
(65 280 ***k*** points in the first Brillouin zone)

$\sim 10^6$ s.p. wavefunctions

- The superfluid density is strongly suppressed $\rho_{\rm S} \ll \rho_n$.
- The superfluid density is not very sensitive to Δ ($\delta\rho_{\rm S}/\rho_{\rm S} \lesssim 4\%$).

Superfluid reservoir and giant pulsar glitches

This challenges the standard model of pulsar glitches.

Chamel, PRL 110, 011101 (2013)

The inferred mass of the Vela pulsar is much lower than expected.

For such stars, the equation of state ($\bar{n} \lesssim 0.23 - 0.33$ fm^{-3}) is fairly well constrained by laboratory experiments.

The superfluid in the crust does not carry enough angular momentum!

Delsate et al., PRD 94, 023008 (2016)

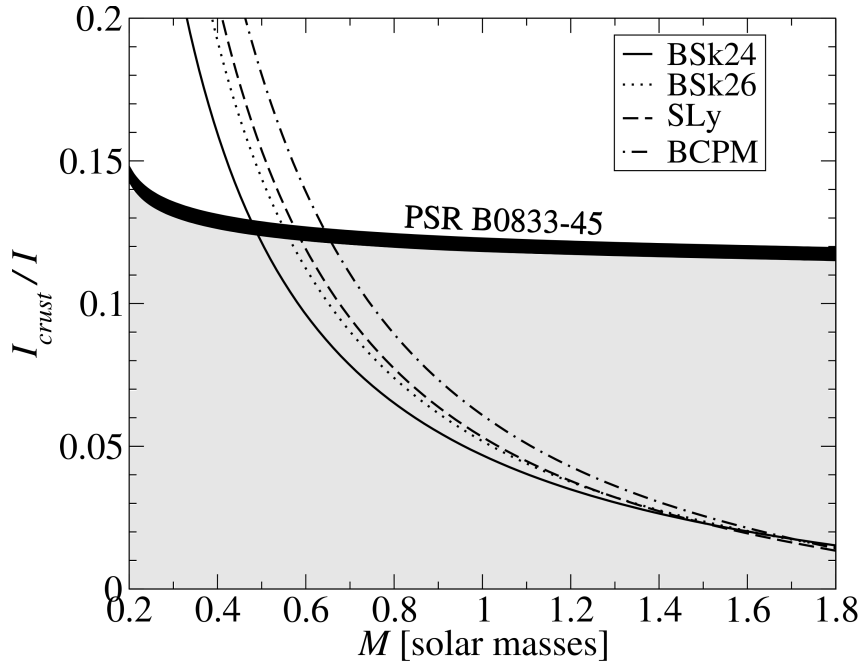

Superfluid reservoir and giant pulsar glitches

This challenges the standard model of pulsar glitches.
Chamel, PRL 110, 011101 (2013)

The inferred mass of the Vela pulsar is much lower than expected.

For such stars, the equation of state ($\bar{n} \lesssim 0.23 - 0.33$ fm^{-3}) is fairly well constrained by laboratory experiments.

The superfluid in the crust does not carry enough angular momentum!

Delsate et al., PRD 94, 023008 (2016)

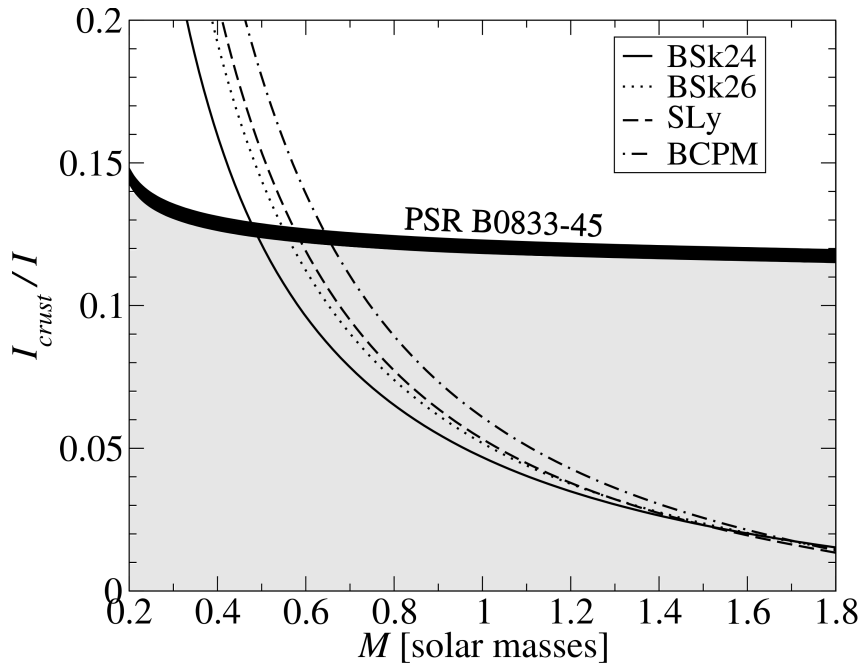

- The superfluid in the core is involved in glitches.
  Sourie & Chamel, MNRAS 493, L98 (2020)
- The suppression of ρ_S is overestimated by the BCS theory.
  Watanabe&Pethick,PRL119, 062701 (2017); *Sekizawa et al.,PRC105, 045807 (2022)*; *Almirante&Urban, PRC109, 045805 (2024)*

Finite superflow and Landau's critical velocity

What happens for finite superflows?

Finite superflow and Landau's critical velocity

What happens for finite superflows?

Ignoring spatial inhomogeneities, the HFB equations can be solved analytically. An **effective superfluid velocity** naturally emerges:

$$\mathbb{V}_{\boldsymbol{q}} \equiv \frac{m_q}{m_q^{\oplus}} \boldsymbol{V}_{\boldsymbol{q}} + \frac{\boldsymbol{I}_{\boldsymbol{q}}}{\hbar}$$

The order parameter Δ_q of the superfluid phase remains unchanged provided $\mathbb{V}_q < \mathbb{V}_{Lq}$, the critical velocity from **Landau's criterion**

$$\mathbb{V}_{Lq} \equiv V_{Fq} \sqrt{\frac{\mu_q}{2\varepsilon_{Fq}} \left[\sqrt{1 + \left(\frac{\Delta_q}{\mu_q} \right)^2} - 1 \right]} \approx \frac{\Delta_q}{\hbar k_{Fq}}$$

This is the generalization to nuclear superfluids of the expression obtained in a single cold Fermi gas

Combescot, Yu Kagan, Stringari, Phys. Rev. A 74, 042717 (2006)

Allard & Chamel, Phys. Rev. C 103, 025804 (2021)

Gapless superfluidity

Superfluidity is not destroyed for super Landau superflow $\mathbb{V}_q \geq \mathbb{V}_{Lq}$, but Δ_q decreases and eventually vanishes for $\mathbb{V}_q = \mathbb{V}_{cq} \approx 1.36\mathbb{V}_{Lq}$. In this intermediate regime, superfluidity becomes gapless:

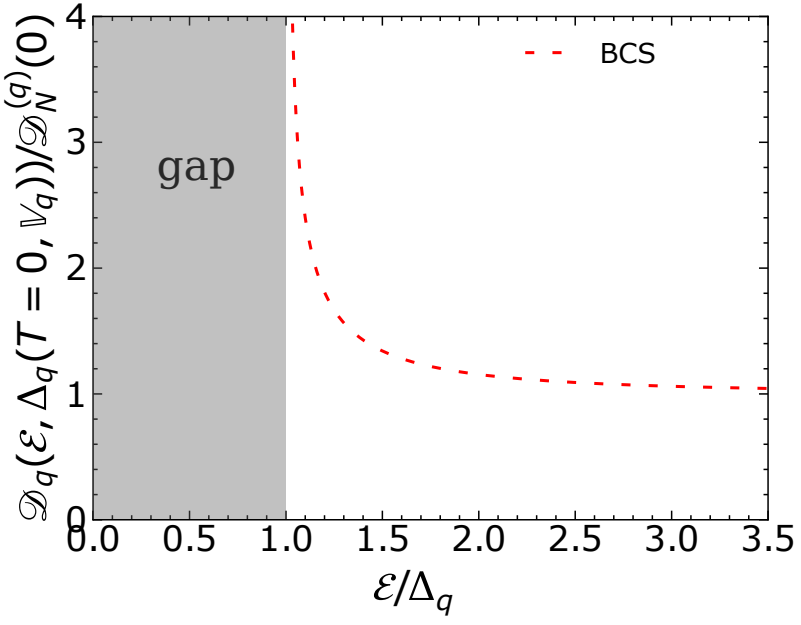

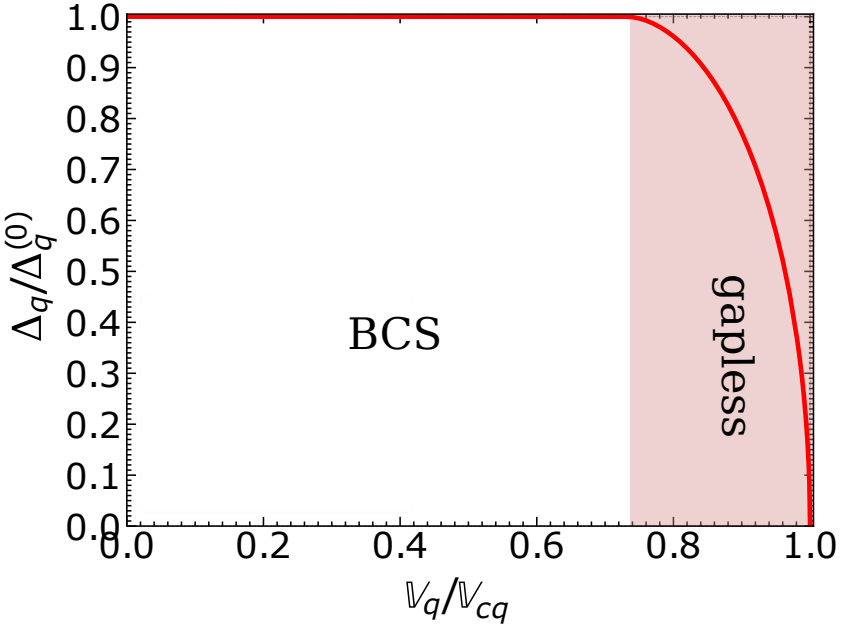

Gapless superfluidity

Superfluidity is not destroyed for super Landau superflow $\mathbb{V}_q \geq \mathbb{V}_{Lq}$, but Δ_q decreases and eventually vanishes for $\mathbb{V}_q = \mathbb{V}_{cq} \approx 1.36\mathbb{V}_{Lq}$. In this intermediate regime, superfluidity becomes gapless:

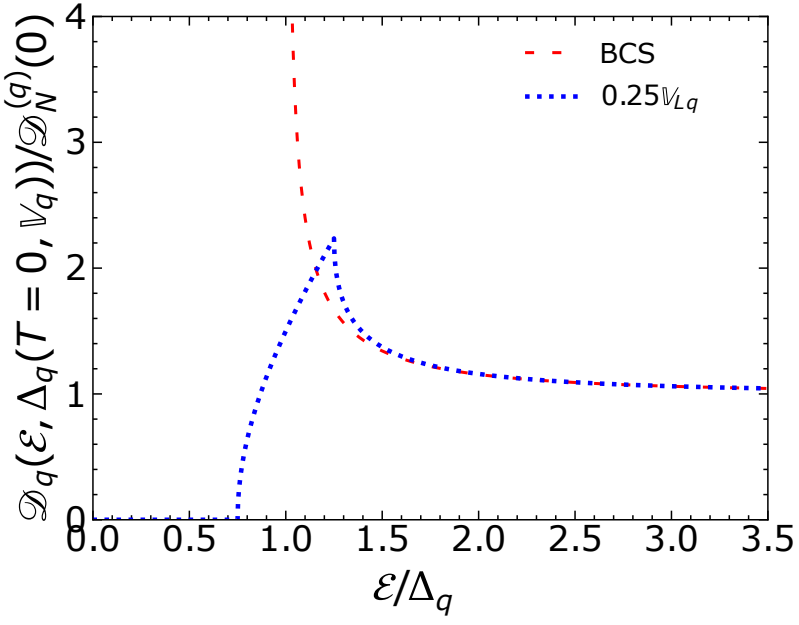

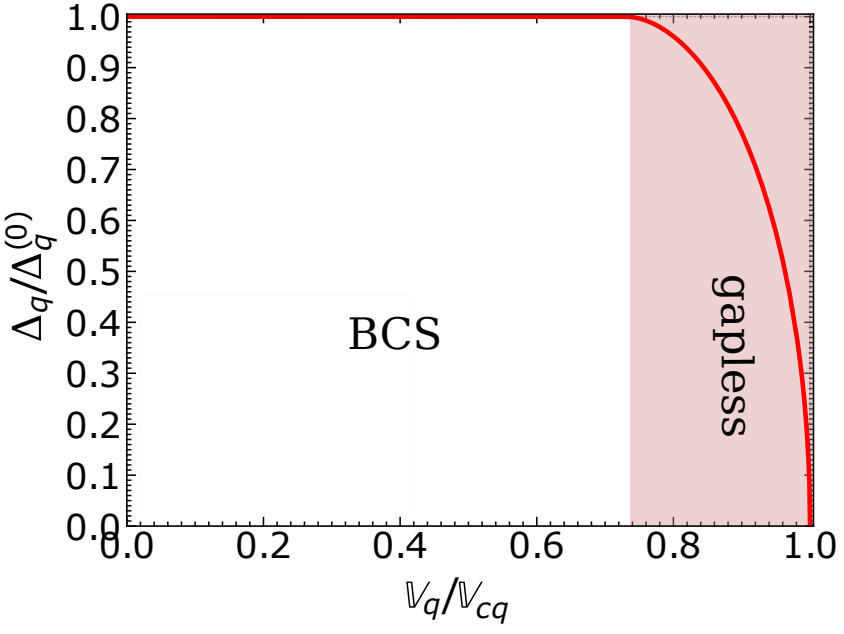

Gapless superfluidity

Superfluidity is not destroyed for super Landau superflow $\mathbb{V}_q \geq \mathbb{V}_{Lq}$, but Δ_q decreases and eventually vanishes for $\mathbb{V}_q = \mathbb{V}_{cq} \approx 1.36\mathbb{V}_{Lq}$. In this intermediate regime, superfluidity becomes gapless:

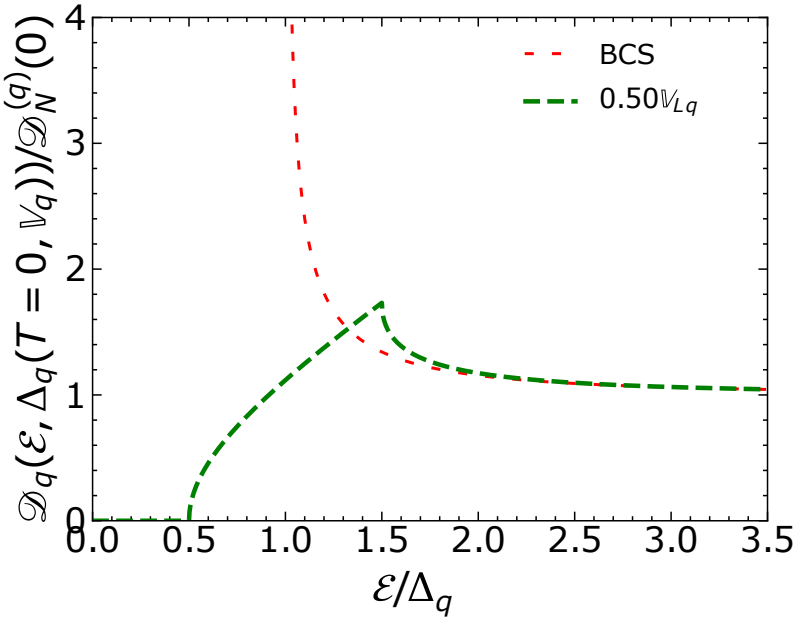

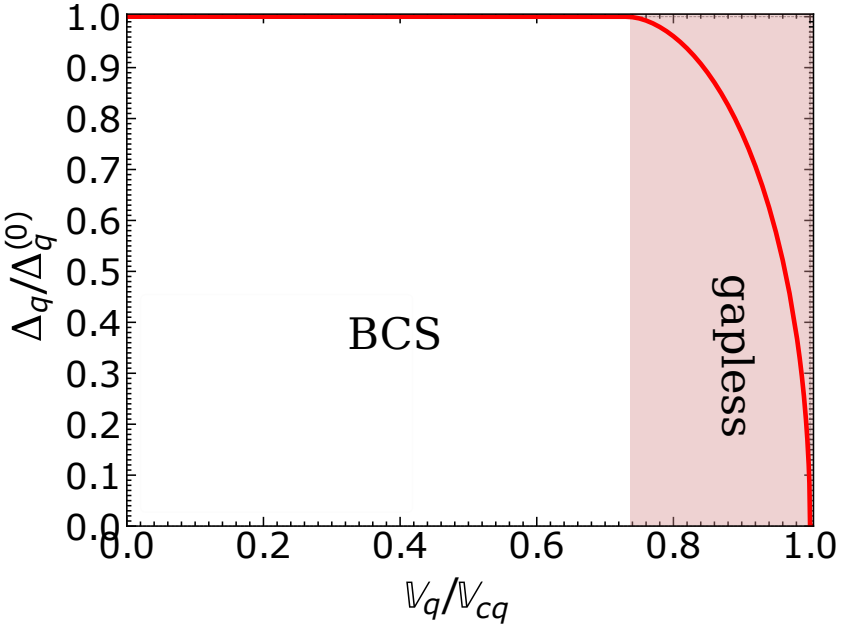

Gapless superfluidity

Superfluidity is not destroyed for super Landau superflow $\mathbb{V}_q \geq \mathbb{V}_{Lq}$, but Δ_q decreases and eventually vanishes for $\mathbb{V}_q = \mathbb{V}_{cq} \approx 1.36\mathbb{V}_{Lq}$. In this intermediate regime, superfluidity becomes gapless:

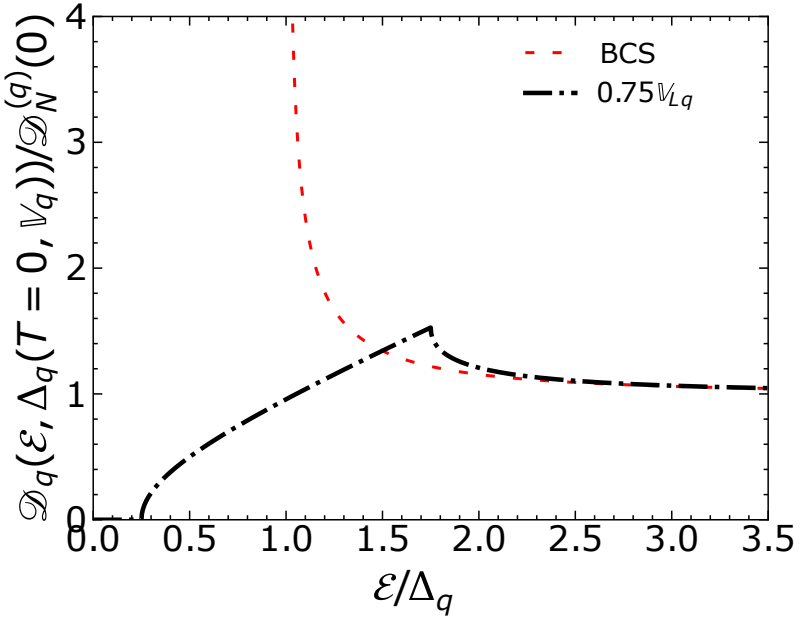

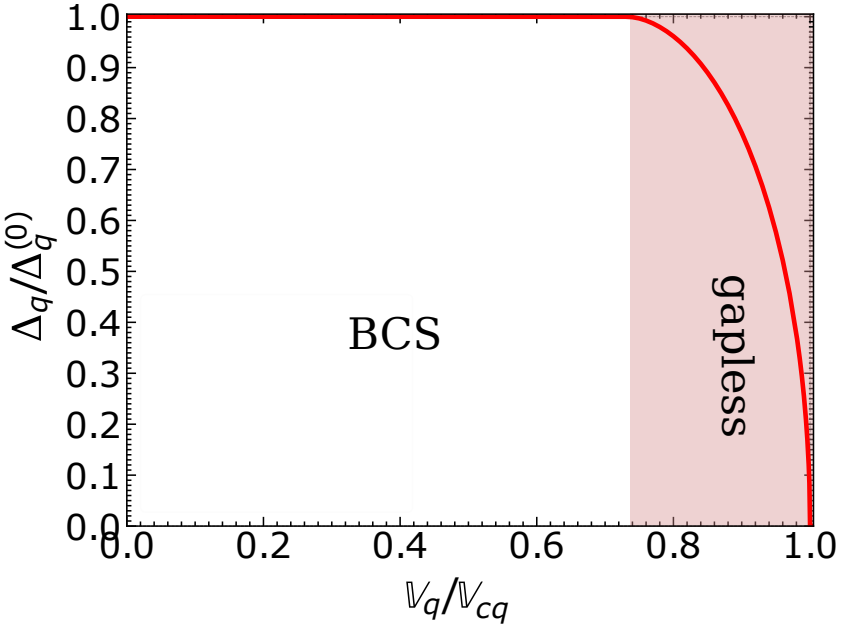

Gapless superfluidity

Superfluidity is not destroyed for super Landau superflow $\mathbb{V}_q \geq \mathbb{V}_{Lq}$, but Δ_q decreases and eventually vanishes for $\mathbb{V}_q = \mathbb{V}_{cq} \approx 1.36\mathbb{V}_{Lq}$. In this intermediate regime, superfluidity becomes gapless:

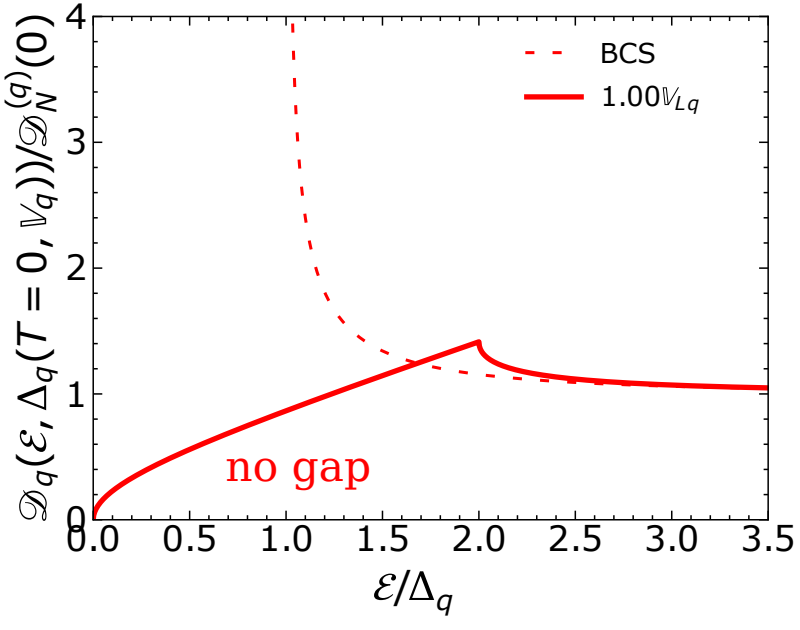

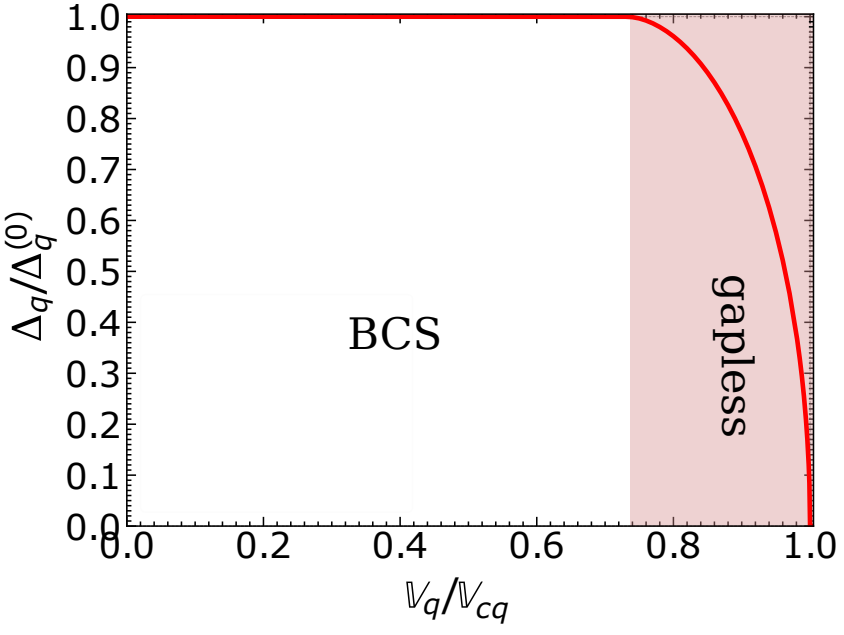

Gapless superfluidity

Superfluidity is not destroyed for super Landau superflow $\mathbb{V}_q \geq \mathbb{V}_{Lq}$, but Δ_q decreases and eventually vanishes for $\mathbb{V}_q = \mathbb{V}_{cq} \approx 1.36\mathbb{V}_{Lq}$. In this intermediate regime, superfluidity becomes gapless:

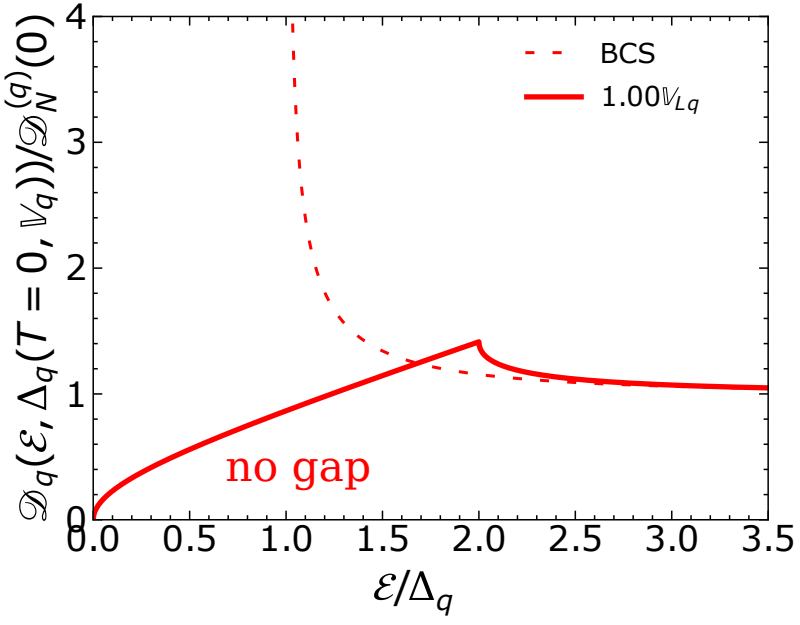

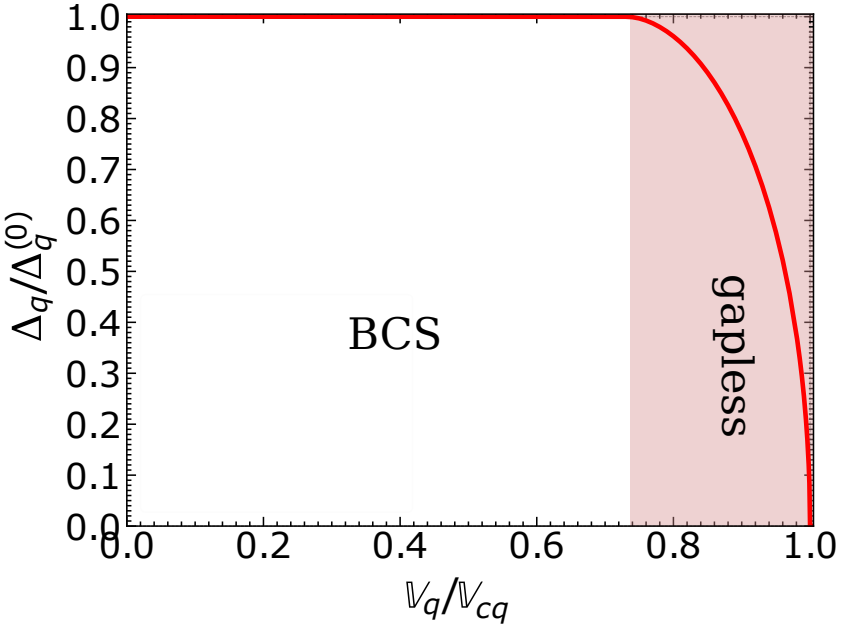

A normal fluid of quasiparticles excitations is present even at $T = 0$.

Allard & Chamel, Phys. Rev. C 103, 025804 (2021); Phys. Rev. C 108, 045801 (2023)

Astrophysical implications

Superfluidity can be probed from the cooling of neutron-star crusts after the end of an accretion episode

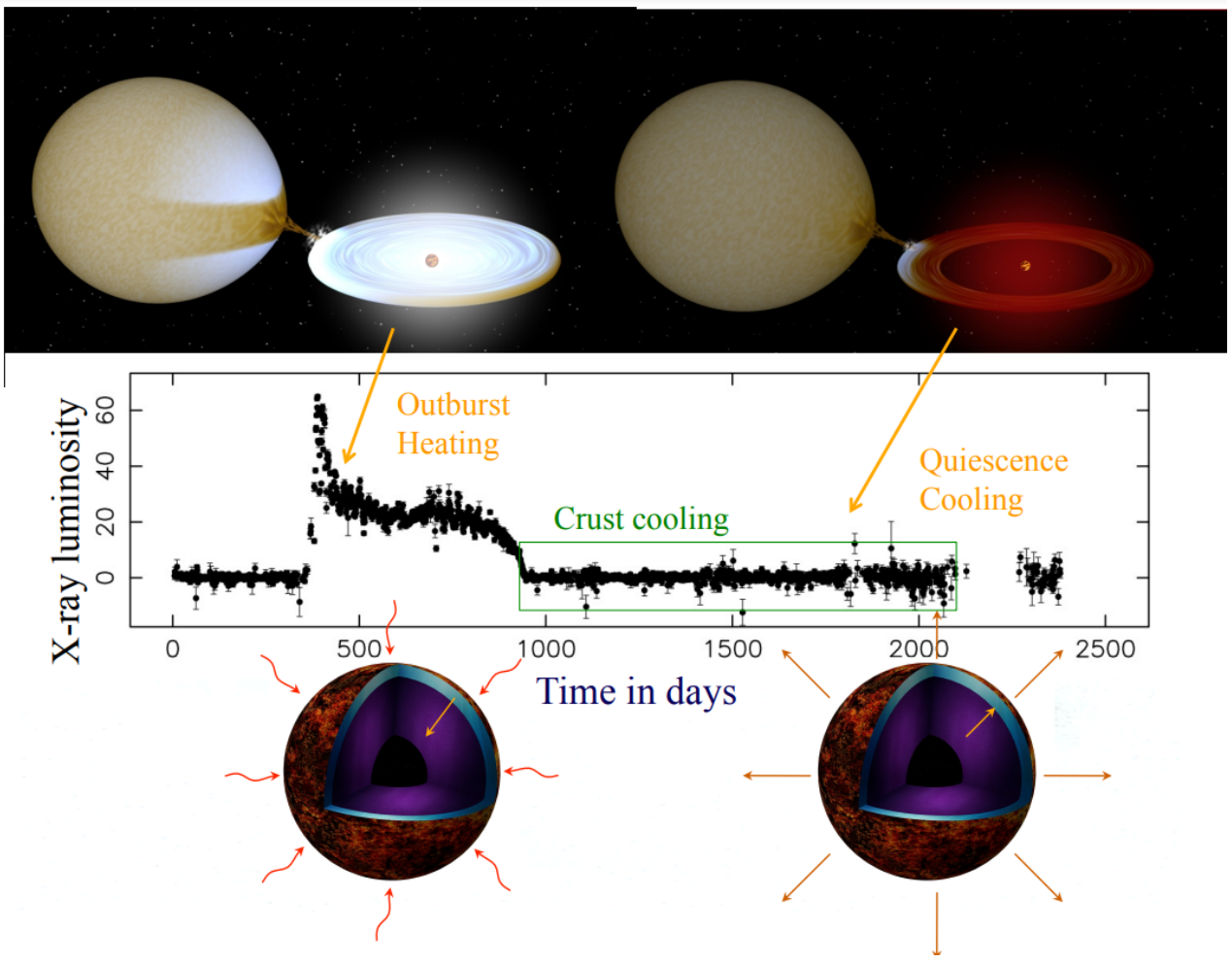

Wijnands, Degenaar, Page, J. Astrophys. Astron. 38, 49, (2017)

Observational puzzles: KS 1731−260

KS 1731−260 appeared **colder than expected** after $\sim$ 3000 days:

Cackett et al., ApJ 722, L137 (2010)

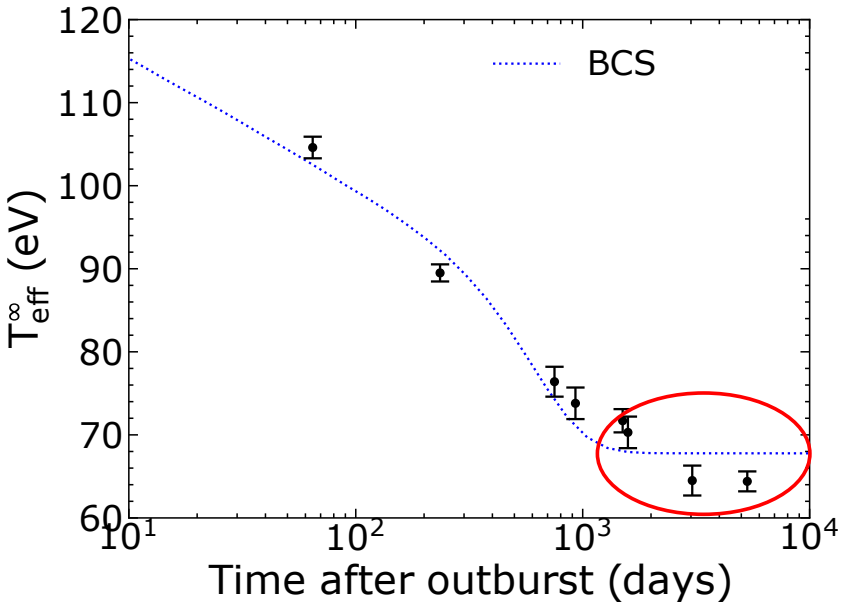

Observational puzzles: KS 1731−260

KS 1731−260 appeared **colder than expected** after $\sim$ 3000 days:

Cackett et al., ApJ 722, L137 (2010)

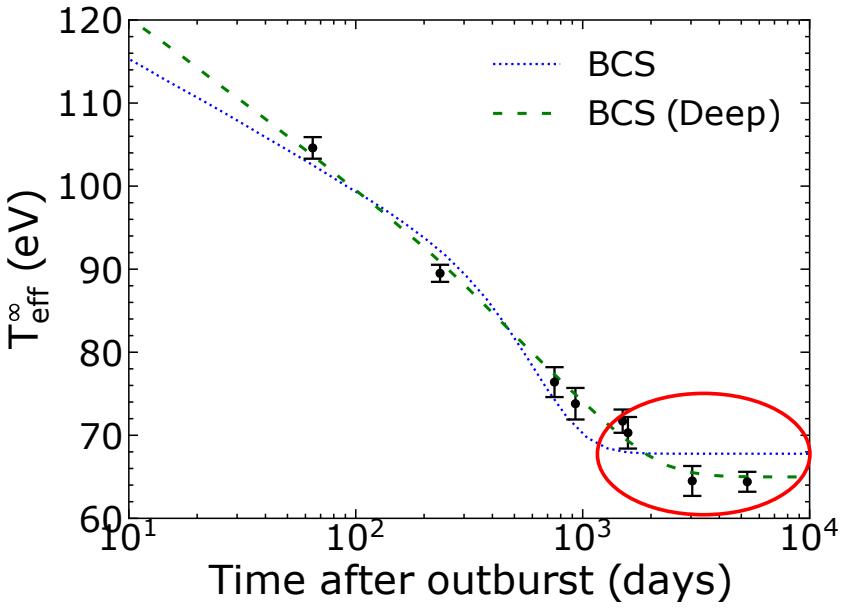

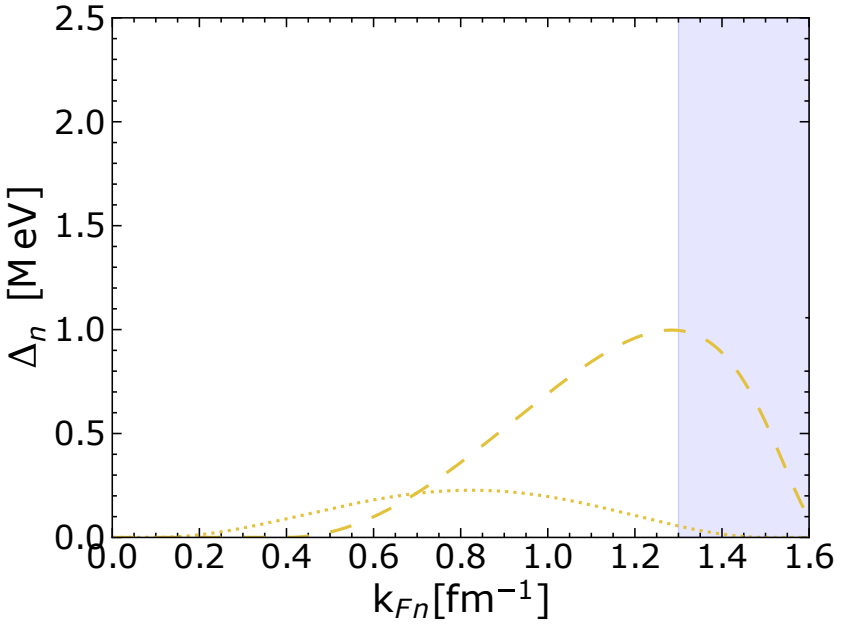

Data could be fitted by **fine tuning the neutron pairing gaps** Δ_n

Turlione et al., A&A 577, A5 (2015)

Observational puzzles: KS 1731−260

KS 1731−260 appeared **colder than expected** after $\sim$ 3000 days:

Cackett et al., ApJ 722, L137 (2010)

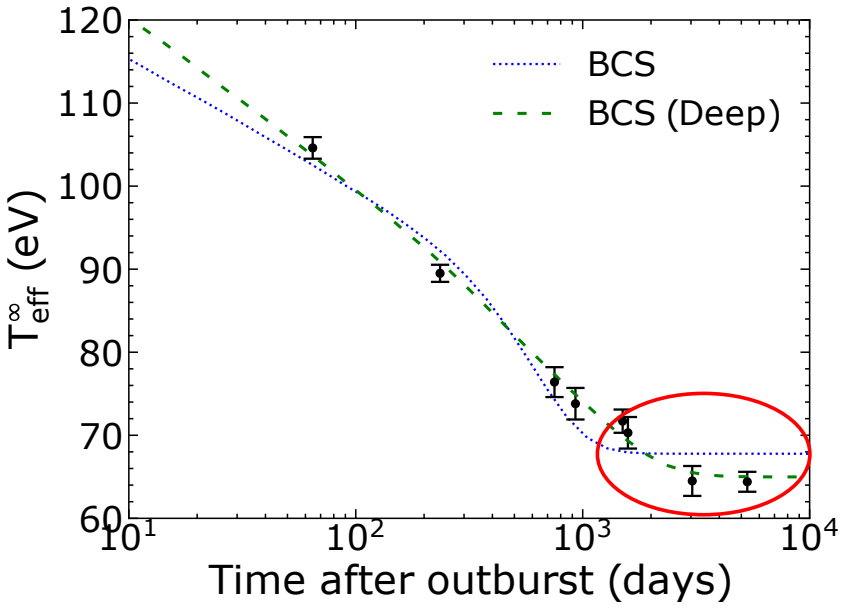

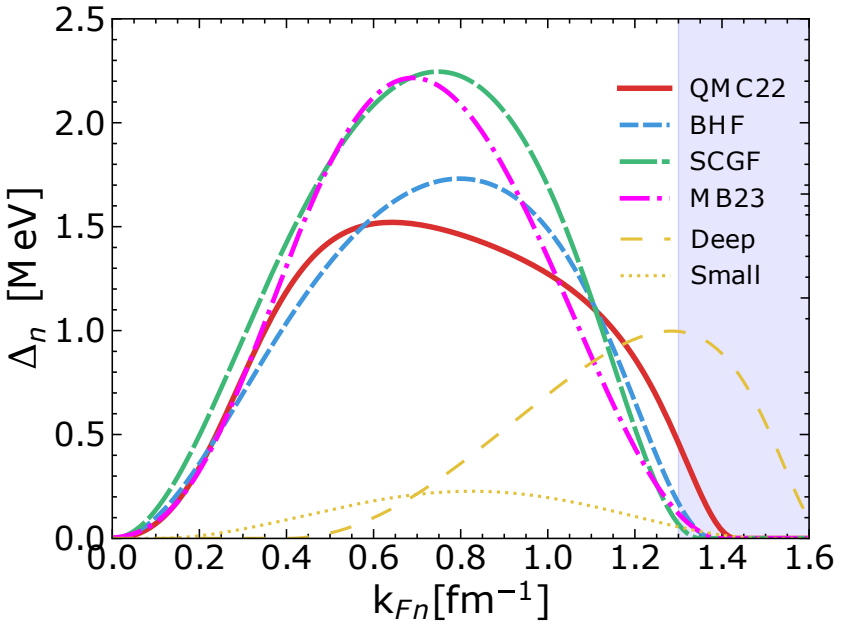

Data could be fitted by **fine tuning the neutron pairing gaps** Δ_n

Turlione et al., A&A 577, A5 (2015)

But these empirical gaps are not compatible with latest microscopic calculations based on different many-body approaches.

Observational puzzles: MXB 1659−29

MXB 1659−29 exhibited an **unexpected late-time cooling**:

Cackett et al., ApJ 774, 131 (2013)

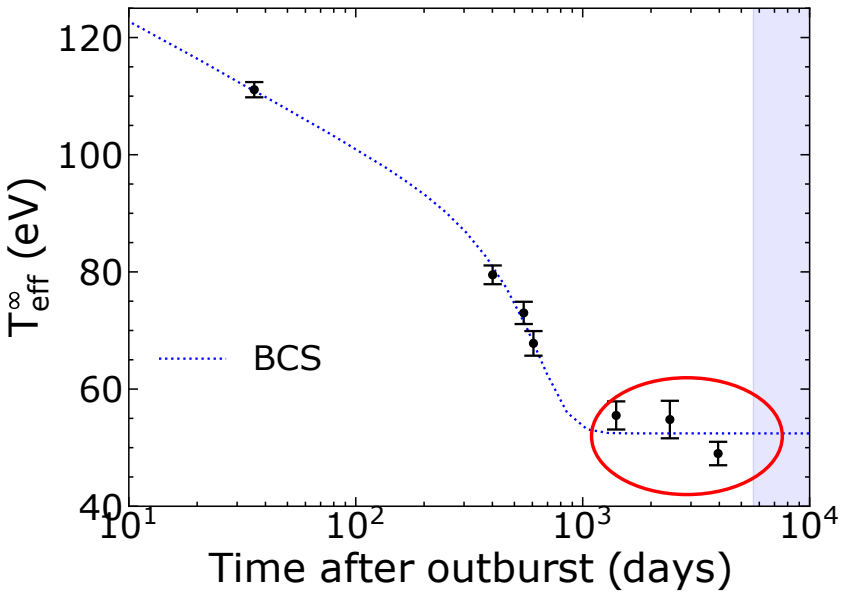

Observational puzzles: MXB 1659−29

MXB 1659−29 exhibited an **unexpected late-time cooling**:

Cackett et al., ApJ 774, 131 (2013)

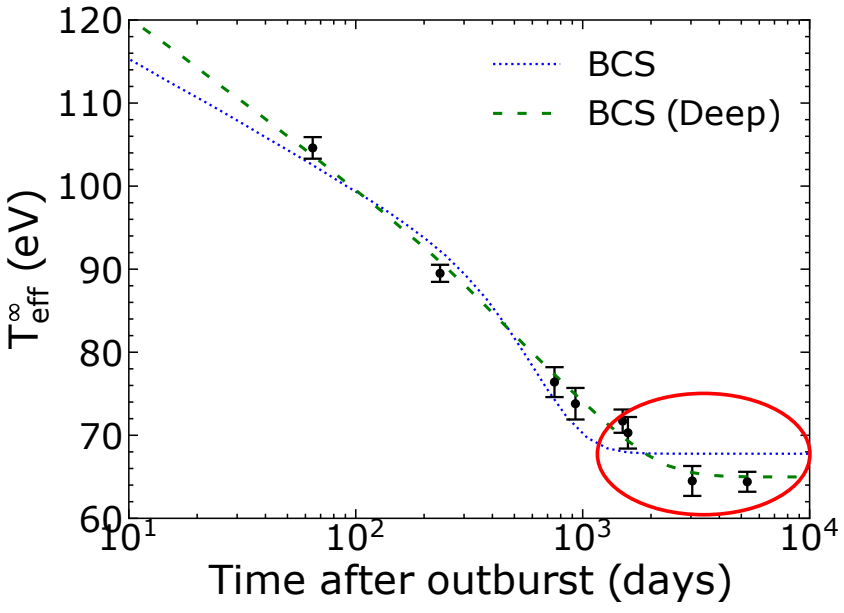

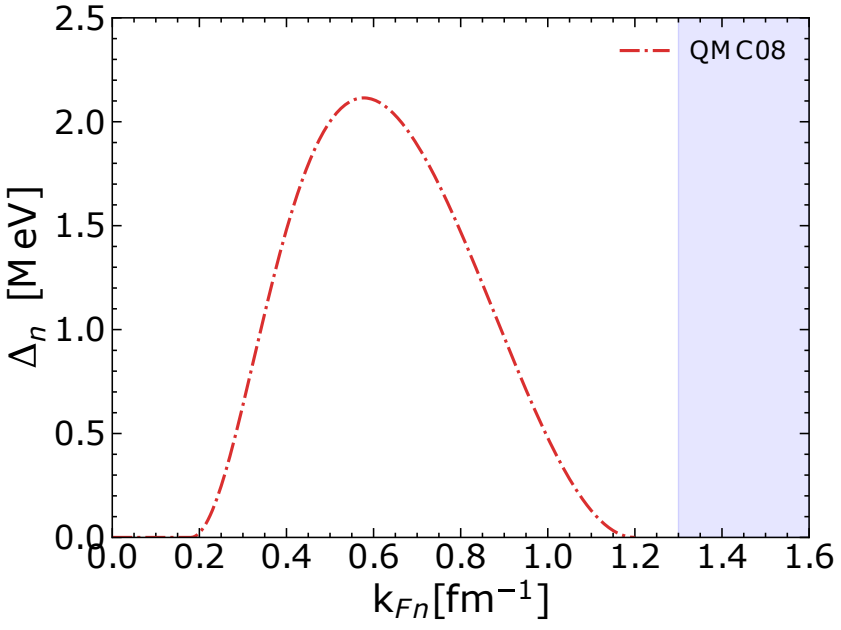

Data could be fitted by **considering the vanishing of neutron pairing gaps** in the densest crustal layers

Deibel et al., ApJ 839, 95 (2017)

Observational puzzles: MXB 1659−29

MXB 1659−29 exhibited an **unexpected late-time cooling**:

Cackett et al., ApJ 774, 131 (2013)

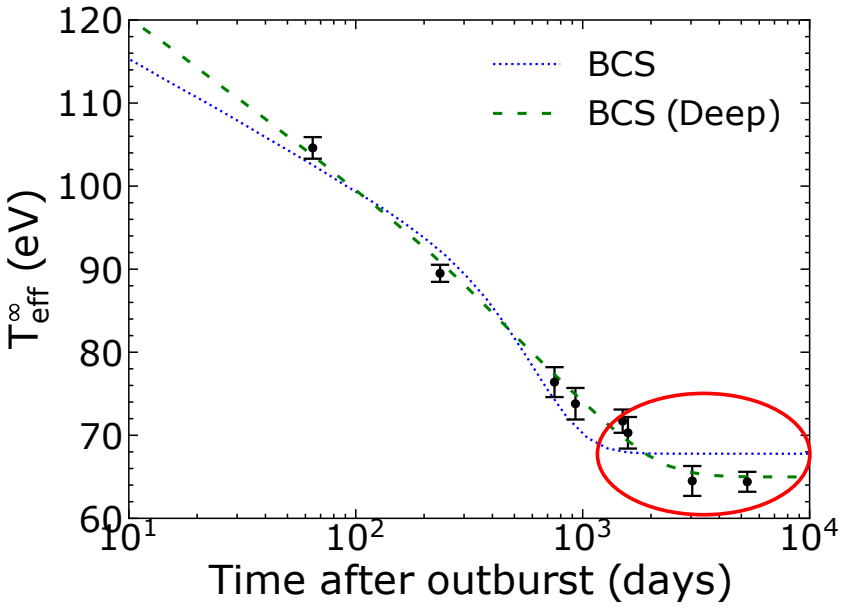

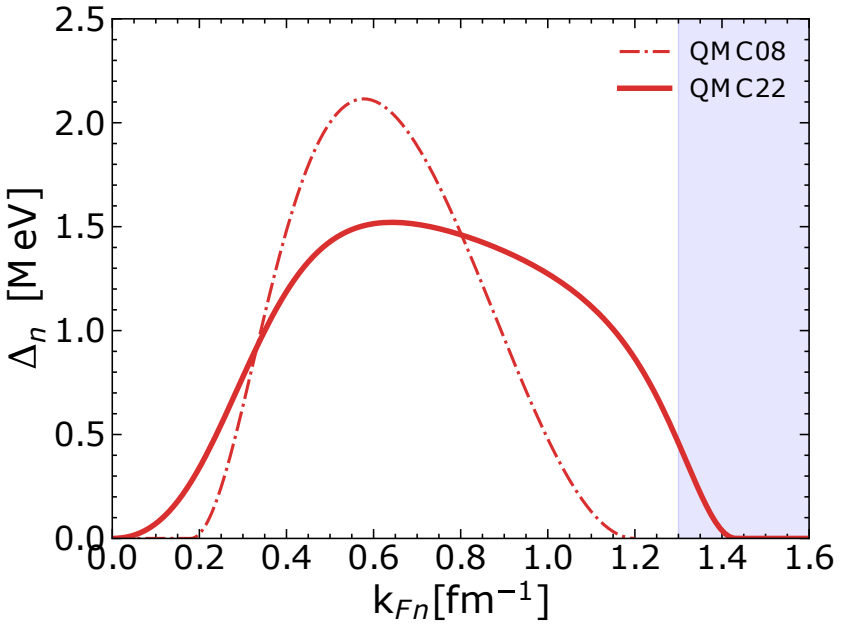

Data could be fitted by **considering the vanishing of neutron pairing gaps** in the densest crustal layers

Deibel et al., ApJ 839, 95 (2017)

But this conclusion is no longer supported by more recent microscopic calculations.

Observational evidence of gapless superfluidity

Within standard cooling models, the thermal relaxation is too fast due to the suppression of the neutron specific heat.

Observational evidence of gapless superfluidity

Within standard cooling models, the thermal relaxation is too fast due to the suppression of the neutron specific heat.

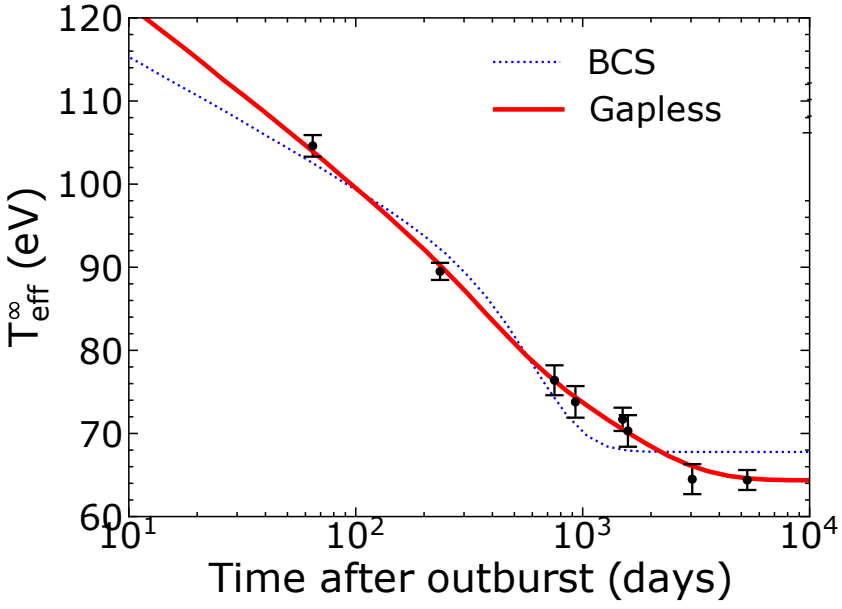

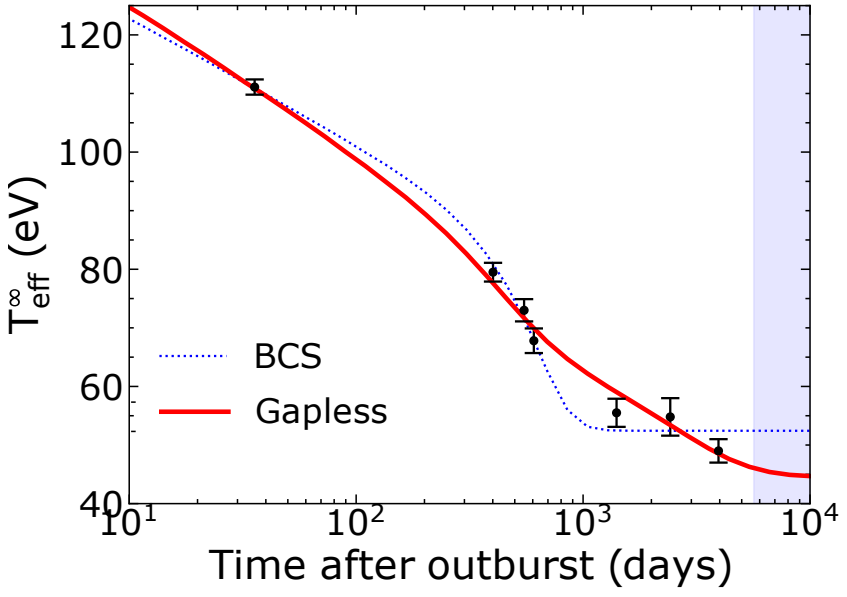

Gapless superfluidity can naturally explain the observed late-time cooling due to the huge enhancement of the neutron specific heat.

Allard & Chamel, PRL in press

Conclusions & Perspectives: Part I

We have studied the existence of nuclear pastas in neutron-star crusts based on precision-fitted nuclear functionals:

- purely semiclassical calculations lead to usual pasta phases
- **with quantum corrections, pastas are strongly disfavored**.

On-going:

- Error assessment and further improvement of ETFSI method
- Full 3D HFB calculations of nuclear pastas (Nikolai Shchechilin)

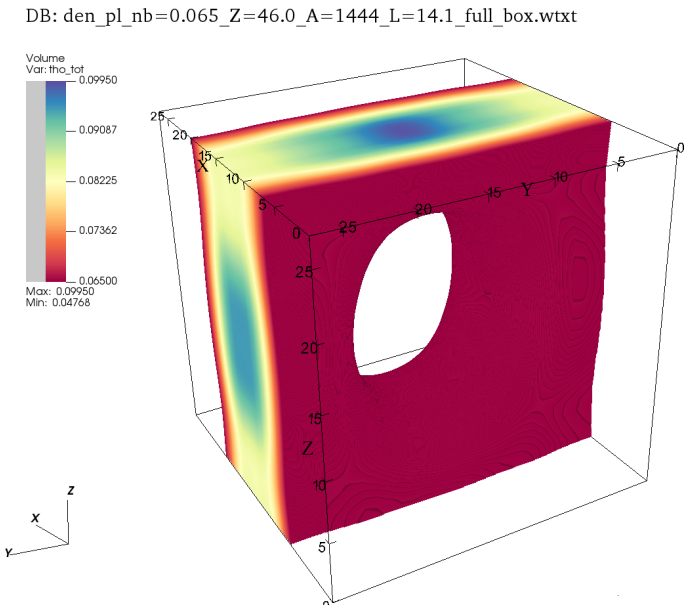

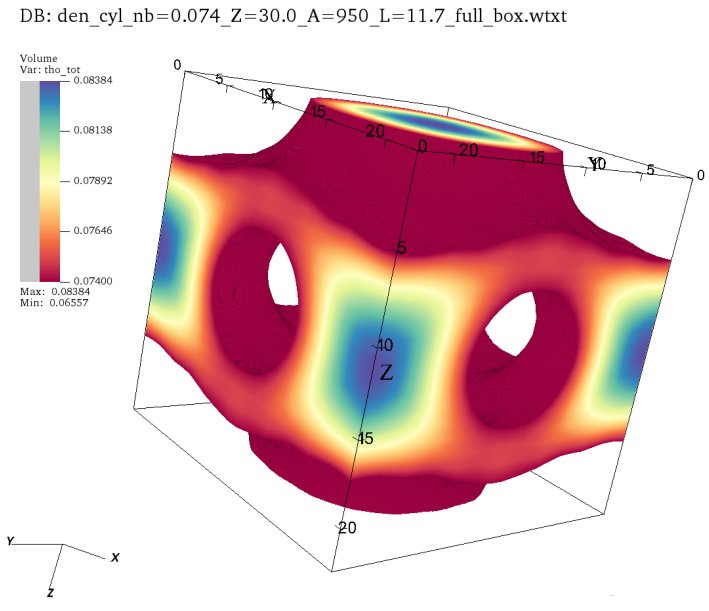

Conclusions & Perspectives: Part II

We have studied neutron superfluidity in neutron-star crusts:

- neutron superfluidity is suppressed due to Bragg scattering
- super Landau superflow naturally explains the observed cooling of transiently accreting neutron stars.

On-going:

- Sensitivity analysis of neutron-star crust cooling (Valentin Allard)
- Full 3D time-dependent HFB calculations of neutron superfluidity (Piotr Magierski, Gabriel Wlazłowski, Daniel Pęcak)

Pęcak et al., arXiv:2403.17499

Unified equations of state

We have constructed **thermodynamically consistent** equations of state for neutron stars:

- isolated neutron stars
  Pearson et al.,MNRAS 481, 2994 (2018)
- magnetars
  Mutafchieva et al., Phys. Rev. C 99, 055805 (2019)
- accreting neutron stars
  Fantina et al., A&A 620, A105 (2018); A&A 665, A74 (2022)

Tables available on CompOSE: `https://compose.obspm.fr/`

Freely available computer codes and data for the outer crust:
`http://doi.org/10.5281/zenodo.3719439`
`http://doi.org/10.5281/zenodo.3839787`

Consistent $^1S_0$ pairing gaps: *Allard&Chamel, Universe 7(12), 470 (2021)*

Gravito-electric and magnetic Love numbers up to $\ell = 5$:
Perot&Chamel,Phys.Rev.C103, 025801 (2021)

Special thank

Collaborative work:

Nikolai Shchechilin, Valentin Allard, Guilherme Grams, Chiranjib Mondal, Wouter Ryssens, Stephane Goriely

John-Michael Pearson

Alexander Potekhin, Andrey Chugunov, Mikhael Gusakov

Piotr Magierski, Gabriel Wlazłowski, Daniel Pęcak